

# Gauge-ball spectrum of the four-dimensional pure U(1) gauge theory

J. Cox, W. Franzki, J. Jersák

*Institut für Theoretische Physik E, RWTH Aachen, Germany*

C. B. Lang

*Institut für Theoretische Physik, Karl-Franzens-Universität Graz, Austria*

T. Neuhaus

*Niels Bohr Institute, Univ. of Copenhagen, Denmark*

P. W. Stephenson

*DESY, Zeuthen, Germany*

---

## Abstract

We investigate the continuum limit of the gauge-ball spectrum in the four-dimensional pure U(1) lattice gauge theory. In the confinement phase we identify various states scaling with the correlation length exponent  $\nu \simeq 0.35$ . The square root of the string tension also scales with this exponent, which agrees with the non-Gaussian fixed point exponent recently found in the finite size studies of this theory. Possible scenarios for constructing a non-Gaussian continuum theory with the observed gauge-ball spectrum are discussed. The  $0^{++}$  state, however, scales with a Gaussian value  $\nu \simeq 0.5$ . This suggests the existence of a second, Gaussian continuum limit in the confinement phase and also the presence of a light or possibly massless scalar in the non-Gaussian continuum theory. In the Coulomb phase we find evidence for a few gauge-balls, being resonances in multi-photon channels; they seem to approach the continuum limit with as yet unknown critical exponents. The maximal value of the renormalized coupling in this phase is determined and its universality confirmed.

---

## 1 Introduction

Since studies of lattice gauge theories began it has been conjectured that the pure  $U(1)$  gauge theory in four dimensions (4D) might possess two continuum limits at the phase transition between the confinement and the Coulomb phases [1,2], provided the transition is of 2<sup>nd</sup> order. The continuum limit depends on the phase in which it is approached. In the confinement phase various gauge-balls (GB) with finite masses, analogous to the glue-balls of pure QCD, as well as a finite string tension  $\sigma$ , are expected. In the Coulomb phase with a massless photon dilute magnetic monopoles might exist, whereas in the confinement phase they condense. These phenomena were clearly observed for a finite lattice cutoff  $1/a$  long ago [3,4]. However, the continuum limit has remained elusive for the subsequent 13 years.

The main reason for this delay has been the two-state signal at the phase transition observed on finite lattices with periodic boundary conditions [5,6]. However, it has recently been demonstrated that if, instead of such toroidal lattices, those with trivial homotopy group are used, the two-state signal disappears for the Wilson action [7], extended Wilson action (defined below) at  $\gamma \leq 0$  [8,9], and the Villain action [10]. Furthermore, in high precision simulations on specially constructed homogeneous spherical lattices, the finite size scaling (FSS) behaviour turned out to be well described by the leading term of the critical behaviour with a non-Gaussian value of the correlation length critical exponent,  $\nu = 0.365(8)$  [8–10].

Within the intrinsic uncertainties of numerical evidence this demonstrates that the phase transition is of second order in some parameter region and the corresponding continuum limit is governed by a non-Gaussian fixed point. The expected continuum limit is thus presumably a nontrivial quantum field theory which is not asymptotically free. Until now no such nonperturbatively defined continuum quantum field theory has been established in four dimensions. Further investigation of this theory is therefore of high theoretical interest.

The use of spherical lattices has been crucial for the study of the model by FSS methods, because this method combines scaling and finite size phenomena. Thus the latter should not be distorted by topological effects. However, once the critical properties are established, there is no urgent need to use such complicated lattices for investigations of the spectrum of the model. The topology of finite lattices of volume  $V$  ought to be irrelevant for the thermodynamic limit,  $V \rightarrow \infty$ , if that is taken before the continuum limit, when the lattice constant  $a \rightarrow 0$ . The restrictions imposed by the two-state signal on toroidal lattices can be avoided by using large  $V$  and choosing the coupling parameters outside the metastability region on these lattices. In fact, fairly precise values of  $\nu = 0.28 - 0.42$  have been obtained by this approach in the

past.

In this work we therefore return to the 4D toroidal lattices and adapt the latest methods of glue-ball measurements in QCD on such lattices to the U(1) gauge group. Since the most recent studies have indicated universality of the scaling behaviour [8–10], we have chosen an action reducing the two-state signal while keeping the autocorrelation time reasonably short: the extended Wilson action at the double-charge coupling  $\gamma = -0.2$ .

We have investigated in both phases on large lattices the correlation functions in 20 channels with the zero momentum and in some channels with the smallest nonzero momentum as well. We have also determined the static potential from the same runs.

In the confinement phase, we have obtained masses  $m_j$  (inverse correlation lengths) in most channels. Within the considered parameter range the finite size effects are negligible. Also the string tension  $\sigma$  has been determined from the values of the potential at the largest separations. We investigate the scaling behaviour of these observables, i.e. their vanishing in lattice units, when  $\beta$ , the standard Wilson coupling, approaches its critical value  $\beta_c$ .

Our main result for the confinement phase in the vicinity of the critical point  $\beta_c$  is the evidence for two groups of GB masses with distinctly different scaling behaviour when the phase transition is approached,  $\tau = |\beta - \beta_c| \rightarrow 0$ . Most of the GB masses, and approximately also  $\sqrt{\sigma}$ , scale proportional to  $\tau^{\nu_{\text{ng}}}$ , the value of the correlation length exponent  $\nu_{\text{ng}}$  being non-Gaussian,

$$\nu_{\text{ng}} = 0.35(3). \tag{1}$$

This agrees with the exponent  $\nu = 0.365(8)$  found in FSS studies on spherical lattices [8–10].

However, the mass of the  $J^{PC} = 0^{++}$  GB scales as  $\tau^{\nu_{\text{g}}}$ , with

$$\nu_{\text{g}} = 0.49(7). \tag{2}$$

This correlation length exponent agrees with the Gaussian value  $\nu = 1/2$ . The critical point, common for both groups, is at

$$\beta_c \simeq 1.1607(3). \tag{3}$$

The errors indicated in the above three equations include both statistical and systematic uncertainties of our results. Since the latter are not independent,

we also give the result for the ratio of both exponents,

$$\frac{\nu_{\text{ng}}}{\nu_{\text{g}}} = 0.71(8). \quad (4)$$

These findings suggest that in the confinement phase two different continuum limits are possible. One is non-Gaussian, in which all states scaling as  $\tau^{\nu_{\text{ng}}}$  are obtained. Numerous GB states with a somewhat degenerate spectrum, as well as the finite and nonvanishing string tension should be expected. Our recent [8–10] and present results suggest that the observables scaling as  $\tau^{\nu_{\text{ng}}}$  correspond to a nontrivial continuum theory which is not asymptotically free. This theory contains a light, possibly massless scalar.

The other continuum limit in the confinement phase, based on scaling like  $\tau^{\nu_{\text{g}}}$ , is presumably Gaussian. Of all the reliably measured GB masses only that of the  $0^{++}$  state has this behaviour.

The Gaussian exponent (2) has not been detected in the finite size scaling approach [8–10]. However, the existence of two eigenvalues of the linearized renormalization group transformation matrix, consistent with the values (1) and (2) of the critical exponents, was observed back in the eighties in Monte Carlo renormalization group studies of the model [11,12]. These exponents can now be interpreted in terms of the scaling of physical observables.

In the Coulomb phase we find evidence that in the vicinity of the phase transition, apart from the massless vector (“photon”) state, also massive states are present. They appear to scale at the phase transition. We identify them as resonances in two-photon and three-photon channels, respectively, with significant finite size effects. As these are not yet fully under theoretical control, the critical exponents could not be determined. Vanishing of the resonance masses when  $\beta_c$  is approached would imply the existence of a continuum limit with some dimensionful parameter in this phase.

In the Coulomb phase we also obtain from the potential the renormalized coupling  $\alpha_{\text{R}} = e_{\text{R}}^2/4\pi$ . The value of this coupling at the critical point  $\beta_c$ ,  $\alpha_{\text{R},c} = 0.19(1)$  is consistent with that in other formulations of the pure compact U(1) gauge theory. This is further support for the conjectured universality of the renormalized coupling of this theory in the Coulomb phase as one approaches the critical point [13–15].

The results are presented as follows: In the next section we define the model and describe its critical properties. In sec. 3 we discuss the results for the static potential in both phases. Technical details about the GB measurements are collected in sec. 4. In sec. 5 we then present the results for the GB masses in the confinement phase. Possible interpretations of their scaling behaviour are discussed in sec. 6. Sec. 7 is devoted to the results of GB measurements in the

Coulomb phase. The conclusions and a long list of interesting open questions are given in sec. 8. The appendix contains tables with more detailed data.

## 2 The pure U(1) lattice gauge theory

### 2.1 Action and phase diagram

We consider pure compact U(1) lattice gauge theory with an extended Wilson action,

$$S = - \sum_P [\beta \cos(\Theta_P) + \gamma \cos(2\Theta_P)]. \quad (5)$$

Here,  $\Theta_P \in [0, 2\pi)$  is the plaquette angle, i.e. the argument of the product of U(1) link variables around a plaquette  $P$ , and  $\beta$  and  $\gamma$  are the single and the double charge representation couplings, respectively. Taking  $\Theta_P = a^2 g F_{\mu\nu}$ , where  $a$  is the lattice spacing, and  $\beta + 4\gamma = 1/g^2$ , one obtains for weak coupling  $g$  the usual continuum action  $S = \frac{1}{4} \int d^4x F_{\mu\nu}^2$ .

This lattice gauge theory has a line of phase transitions between the strong coupling confinement phase and the weak coupling Coulomb phase. Its position for the Wilson action ( $\gamma = 0$ ) is  $\beta_c \simeq 1.011$  [6], whereas for  $\gamma = -0.2$  it is given in (3). For  $\gamma \geq +0.2$  the transition is clearly of 1<sup>st</sup> order, weakening with decreasing  $\gamma$  [16,6].

The recent studies on spherical lattices strongly suggest that the order changes at  $\gamma = \gamma_0 \simeq 0$ ,  $\gamma_0$  probably being slightly positive, and is of 2<sup>nd</sup> order for  $\gamma \leq \gamma_0$  [8,9]. With decreasing  $\gamma$  the 2<sup>nd</sup> order transition further weakens in the sense that the specific heat peak decreases for fixed lattice size and the autocorrelation time increases [9]. The scaling behaviour of bulk quantities is universal at least in the range  $-0.5 \leq \gamma \leq 0$ .

On toroidal lattices the disturbing two-state signal weakens with decreasing  $\gamma$ , but is present at least until  $\gamma = -0.5$  [6]. For even smaller  $\gamma$  the large autocorrelation time makes simulations prohibitively expensive. Thus on the toroidal lattices the two-state signal on the critical line cannot be avoided.

### 2.2 Some earlier studies

It has been suggested [6] that the point  $\gamma_0$  is a tricritical point (TCP). However, we would like to point out that the TCP's are *not* defined merely as points

on phase transition lines where the change between the 1<sup>st</sup> and 2<sup>nd</sup> order takes place. More is required: in a parameter space enlarged by an external coupling to the order parameter three critical lines should emerge from the TCP [17,6]. This results in TCP's being associated with tricritical exponents different from the critical ones on the emerging critical lines. Up to now there has been no evidence that the point  $\gamma_0$  in the pure compact U(1) gauge theory is really a TCP, because the other critical lines are not known. The problem is in finding the suitably enlarged coupling space while only nonlocal order parameters distinguishing between the confinement and Coulomb phases, like the string tension or the photon mass, exist. This problem may be specific for gauge theories. It makes an interpretation of the two observed scaling laws in terms of critical and tricritical scaling behaviour uncertain.

Various investigations of the scaling behaviour of the model by analytic means [18], the finite size scaling analysis [16,19] and the Monte Carlo renormalization group (MCRG) method [11,12,20] found the correlation length exponent  $\nu$  to be in the range  $\nu \simeq 0.28 - 0.42$ . In some MCRG studies the existence of a second value of this exponent, consistent with  $\nu = 0.5$ , was observed [11,12] suggesting that one of these exponents is tricritical and the other critical. In ref. [11] the tricritical value was suggested to be  $\nu = 0.5$ , whereas in refs. [12] the assignment was opposite, the tricritical exponent being the non-Gaussian one. Recently, evidence has been provided, that in the coupling space enlarged by monopole coupling, a second order phase transition with non-Gaussian critical exponents may be observed [21].

Because of the doubts as to whether a continuum limit can be obtained, calculations of the spectrum of the model are sporadic. The massless photon in the Coulomb phase was observed in various studies [4,22–25] and the presence of several gauge-balls in both phases was indicated in [4]. In [23,24] the  $1^{--}$  gauge-ball, the “massive photon” in the confinement phase was found and in [23] its scaling investigated and found to be consistent with  $\nu = 0.33$ . The monopole mass was measured in the Coulomb phase in a dual formulation of the theory [26]. To our knowledge its scaling behaviour has not yet been studied.

### *2.3 Overview of our measurements*

Motivated by the recent progress in understanding the continuum limit, in the present work we investigate the spectrum and its scaling behaviour. Our choice of  $\gamma = -0.2$  is a compromise between the requirements of minimizing both the two-state signal and the autocorrelation time.

In the simulations we have used a vectorized three-hit Metropolis algorithm

$\beta$	$8^3 16$	$10^3 20$	$12^3 24$	$14^3 28$	$16^3 32$	$18^3 36$	$20^3 40$
1.100	-	-	6.0	-	5.2	-	-
1.130	8.0	-	6.0	-	5.7	-	-
1.135	-	-	-	-	4.5	-	-
1.140	5.0	-	6.0	-	6.8	-	-
1.145	-	-	-	-	6.6	-	-
1.150	16.0	-	9.0	-	7.5	-	-
1.152	5.0	-	5.0	-	3.6	-	-
1.154	-	-	9.0	-	6.4	-	2.4
1.156	-	-	2.0	-	6.4	-	1.6
1.158	-	-	-	-	6.1	-	2.0
1.159	-	-	-	-	1.0	-	13.7
1.160	-	-	-	-	-	-	0.6
1.161	10.0	4.0	8.0	1.0	6.0	-	1.6
1.162	5.0	4.0	4.0	1.0	3.0	1.6	1.2
1.165	52.0	4.0	10.0	1.0	14.0	0.8	2.4
1.170	44.0	22.0	14.0	9.4	16.7	2.5	3.0
1.180	14.0	4.0	4.0	1.0	10.0	0.8	1.6
1.190	-	-	-	-	2.0	-	-
1.200	5.0	-	4.0	-	5.0	-	1.0

Table 1

List of our data in the confinement (upper part) and Coulomb phases. The numbers in the table are the numbers of measurements in multiples of 1000.

with acceptance around 50% at every hit. The measurements have been performed every 25 sweeps. The used lattice sizes  $L_s^3 L_t$ ,  $L_t = 2L_s$ , are listed in table 1. In the confinement phase the presented data have been obtained on the  $L_s^3 L_t = 16^3 32$  and  $20^3 40$  lattices (smaller lattices being used only for explorative calculations). In the Coulomb phase the lattice size has been varied in a broad range.

In table 1 we list the  $\beta$  values at which the measurements were made. The point  $\beta = 1.100$  turned out to be too deep in the confinement phase to allow reliable measurements of the masses. At  $\beta = 1.160$  an indication of phase flips was observed even on our largest lattice. These two points have therefore been excluded from the data analysis, leaving 10 points  $\beta = 1.130 - 1.159$  in the confinement phase. In the Coulomb phase the data have been collected at 7

points. All data in the vicinity of  $\beta_c$  have been checked for absence of any indication of phase flips in the time evolution of the plaquette energy.

The calculation of the GB masses at many  $\beta$  points, required for the study of their scaling behaviour, limited the statistics at any given  $\beta$ . This made it difficult to distinguish GB states from background in channels with weak GB signal. To improve this situation we have accumulated substantially higher statistics for at least one point,  $\beta = 1.159$  on the  $20^3 40$  lattice. This is the point closest to  $\beta_c$  that still has no phase flips. This allows us to determine the GB masses in channels with weaker signal with higher reliability at least at one  $\beta$ .

As listed in table 1, we have typically accumulated several thousand statistically independent gauge field configurations. We have made two sorts of measurements. The expectation values of the rectangular Wilson loop operators  $W_{R,T}$  with temporal extension  $T$  and extension  $R$  in any of the spatial directions have been determined. All Wilson loops of sizes  $R = 1, \dots, L_s/2$  and  $T = 1, \dots, L_t/2$  have been considered. From this we have obtained the static potential essentially by standard methods.

Our main task, the measurement of the GB masses in various channels at various  $\beta$ , has been performed by adopting the latest methods of glue-ball measurements in pure gauge lattice QCD to the U(1) gauge group. We have followed [27,28] in implementing the techniques of smearing and diagonalization of the correlation matrices. A more detailed description is given in sec. 4. The effective energies  $\epsilon_j(t)$  in various GB channels  $j$  with zero and, in some cases, smallest nonzero lattice momentum have been obtained at various distances  $t$ . The GB masses  $m_j$  have been obtained from the plateaus of these energies where possible. In some channels with weak GB signal  $\epsilon_j(t)$  at only one  $t$ ,  $t = 1$  could be used, giving at least an estimate of the GB mass. In this procedure the standard lattice dispersion relation has been used.

The lattice calculations provide static potential  $V(R)$ , string tension  $\sigma$ , and masses  $m_j$  in the lattice units. To give these observables in physical units, e.g.  $m_j^{\text{phys}} = m_j/a$ , it is necessary to specify the value and the vanishing of the lattice constant  $a$ . As several scenarios for the continuum limit  $a \rightarrow 0$  must be considered, we postpone this issue to sec. 6 and until then use the lattice units only.

Simultaneously with the above measurements we have also determined various fermionic observables in the quenched approximation. This is aimed at a study of the U(1) theory with staggered fermions and will be published separately [29].



### 3 Static potential

#### 3.1 Measurement of the static potential

In the static potential analysis we include Wilson loop expectation values whose noise to signal ratio is smaller than 20% of the expectation value itself. Typically we observe that Wilson loop expectation values of magnitude 0.0001 and larger are measurable within this threshold, entirely independent of  $\beta$ .

The potential  $V(R)$  between static charges is defined as

$$V(R) = \lim_{T \rightarrow \infty} \frac{1}{T} \ln \langle W_{R,T} \rangle. \quad (6)$$

For finite systems it must be specified in a suitable way.

In the confinement phase the Wilson loop expectation values decay rapidly with increasing  $T$ . To extend the usable  $T$  interval we use the Ansatz

$$\langle W_{R,T} \rangle = C(R)e^{-V(R)T} + C_1(R)e^{-V_1(R)T}, \quad V(R) < V_1(R), \quad (7)$$

at fixed  $R$ . This allows for two leading eigenvalues in the transfer matrix representation of the gauge invariant correlation functions. When compared to the data this truncation appears to be a reasonable approximation. The four-parameter fit at each  $R$  is performed solely for those values of  $R$  where at least 6 data points are below the 20 percent threshold in a  $T$ -interval starting with  $T = 1$ . We find that  $V_1(R)$  exceeds the static potential  $V(R)$  by a factor of about 2 throughout the confinement phase. At  $\beta = 1.130$ , the data point deepest in the confinement phase, we are only able with this method to determine the static potential at distances  $R = 1, 2, 3, 4$ . The situation gradually improves as the critical point is approached. At  $\beta = 1.159$ , the data point closest to criticality, we were able to determine the static potential at distances  $1 \leq R \leq 7$ . We have checked that the values of  $V(R)$  obtained in this way are consistent with those obtained by using the  $T \geq R$  loops only and setting  $C_1(R) = 0$ .

In the Coulomb phase the Wilson loops of the considered sizes are much better measurable. There a fit to the form (7) with  $C_1(R) = 0$  for values of  $T \geq 8$  unambiguously determines the static potential for  $1 \leq R \leq 8$  on  $16^3 32$  lattice.

### 3.2 Confinement phase

In the confinement phase we are primarily interested in the string tension  $\sigma$  and its scaling behaviour. The string tension is defined through the asymptotic behaviour of the potential  $V(R) \propto \sigma R$  as  $R \rightarrow \infty$ . In order to extract  $\sigma$  at the available distances  $R$ , a reliable parameterization of the short distance part of the potential would be of much help, similar to lattice QCD. In the U(1) theory we face a serious obstacle: the lack of theoretical knowledge of the potential at short distances in the strongly interacting theory which is not asymptotically free.

We have experimented with various fits to the potential on the whole available  $R$ -interval, parameterizing the short distance behaviour of the potential in several ways. The lattice Coulomb potential of a massless exchange particle, as well as the lattice Yukawa potential of a massive exchange particle were considered. At the available distances these Ansätze influence the values of  $\sigma$  significantly. This effect is at the 10 percent level for our smallest  $\beta$ -values, where the potential is only known at few  $R$ -values, and is less pronounced, at the level of a few percent, close to the critical point. This is so also if the gradient of the potential, the force, is considered. In summary, we cannot avoid a dependence of the fitted string tension values on the Ansatz for the short range part of the potential if all the data for  $V(R)$  are fitted. As this systematic error decreases when the critical point is approached, it distorts the scaling behaviour of  $\sigma$  determined in such a way.

In this situation we expect that a straight line fit to the potential for the largest  $R$ -values results in a less ambiguous and model independent determination of the string tension. For the final determination of  $\sigma$  at all the  $\beta$  values considered we used the potential data at the 3 largest  $R$  values with  $V(R)$  being measurable in the sense described above. In table 2 the obtained values of the string tension in the confinement phase are listed.

The square root of the string tension  $\sqrt{\sigma}$  is expected to scale like a mass. We fit the string tension data using the critical value  $\beta_c = 1.1607$  which is obtained below from the scaling of the GB spectrum. Recalling that our string tension determination is less affected by systematic uncertainties close to the phase transition we restrict the fit to  $1.14 \leq \beta < \beta_c$ . The fit to the scaling form

$$\sqrt{\sigma} = c_\sigma \tau^{\nu_\sigma} \tag{8}$$

results in the exponent value  $\nu_\sigma = 0.35(2)$  and a  $\chi^2/N_{\text{DF}}$ -value for the fit of about 1.9. We test the stability of the fit by the omission of further data points and obtain  $\nu$ -values scattering in a 10 percent interval around the quoted value.

$\beta$	$\sigma$	
	$16^3 32$	$20^3 40$
1.130	0.268(6)	
1.135	0.244(5)	
1.140	0.226(2)	
1.145	0.178(4)	
1.150	0.137(6)	
1.152	0.109(10)	
1.154	0.118(11)	0.139(15)
1.156	0.086(14)	0.082(13)
1.158	0.066(9)	0.062(17)
1.159		0.028(13)

Table 2

Values of the string tension  $\sigma$  in the confinement phase.

The square root of the string tension data and the fit are displayed in fig. 1a. Within the present numerical and systematic uncertainties we conclude that the string tensions scaling behaviour is consistently described by the non-Gaussian exponent  $\nu_\sigma = \nu_{ng}$ .

### 3.3 Coulomb phase

The static potential in the Coulomb phase is well known to be dominated by the exchange of the massless photon. Its determination and a confirmation of its Coulomb form is a spin-off of our study of the spectrum in this phase. Nevertheless, it is of interest to determine the maximal renormalized coupling at  $\gamma = -0.2$ , as this has not been done before.

An appropriate representation of the lattice Coulomb potential  $V_{L,C}$  is obtained by the lattice Fourier transform of a massless bosonic propagator. It has the form

$$V_{L,C}(R) = \frac{4\pi}{L_s^3} \sum_{\vec{k} \neq 0} \frac{e^{i\vec{k}_1 R}}{\sum_{j=1}^3 2(1 - \cos(k_j))}, \quad k_j = 0, \frac{2\pi}{L_s}, \dots, \frac{2\pi(L_s - 1)}{L_s}. \quad (9)$$

We have fitted the static potential at seven  $\beta$ -points in the Coulomb phase with the form

$$V(R) = -\alpha_R V_{L,C}(R) + \sigma R + C \quad (10)$$

$\beta$	$L_s^3 L_t$	$\alpha_R$
1.161	20 <sup>3</sup> 40	0.180(5)
1.162	20 <sup>3</sup> 40	0.186(3)
1.165	16 <sup>3</sup> 32	0.179(4)
1.170	16 <sup>3</sup> 32	0.169(3)
1.180	16 <sup>3</sup> 32	0.162(2)
1.190	16 <sup>3</sup> 32	0.157(2)
1.200	16 <sup>3</sup> 32	0.152(2)

Table 3

Values of the renormalized fine structure constant  $\alpha_R$  in the Coulomb phase.

and obtain a good description of the potential. The coefficient  $\sigma$  is consistent with zero within error bars, confirming the vanishing of the string tension in the Coulomb phase. We therefore omit the linear term altogether in the determination of the renormalized fine structure constant  $\alpha_R$ . The values of  $\alpha_R$  grow when the critical point is approached. Our data are collected in table 3.

Based on the analogy between the low temperature (small coupling) expansions of the  $D = 2$  XY spin model in its spin-wave phase, and of the compact U(1) gauge theory in the Coulomb phase, one expects [14] that the renormalized fine structure constant behaves according to

$$\alpha_R(\beta) = \alpha_{R,c} - A_\alpha(\beta - \beta_c)^\lambda, \quad \beta > \beta_c. \quad (11)$$

At the critical point a finite value of  $\alpha_{R,c}$  has been predicted and it has been suggested that this value might be universal [13,14]. This is in complete analogy to the  $D = 2$  XY model, where the corresponding coupling of the 2-dimensional analog of the Coulomb potential has the critical value 1/4.

Previous simulations [15] of the model with the Wilson and Villain actions in the Coulomb phase showed consistency between the data and (11): for both actions obtained the value  $\alpha_{R,c} \simeq 0.20$  with an error about 0.02.

In order to determine  $\alpha_{R,c}$  we extrapolate the values of  $\alpha_R$  obtained at non-critical  $\beta$  values in the Coulomb phase to  $\beta_c$  via (11). We have used the value for the critical coupling  $\beta_c$ , as determined by the scaling of the gauge ball spectrum. With three free parameters  $\alpha_{R,c}$ ,  $A_\alpha$  and  $\lambda$  we have obtained

$$\alpha_{R,c} = 0.19(1) \quad , \quad \lambda = 0.5(2) \quad (12)$$

with  $\chi^2/N_{DF} = 0.9$ . We find that  $\alpha_{R,c}$  is quite well determined by this extrap-

olation within the Coulomb phase (cf. fig. 1b).

An alternative determination of the renormalized fine structure constant at  $\beta_c$  can be obtained by assuming that the short range properties of the static potential are smooth at the critical point. Thus in the vicinity of the critical point it is sensible to define  $\alpha_R$  from the short range part of the static potential in the confinement phase too;  $\alpha_{R,c}$  can then be obtained by interpolation. This gives results in agreement with (12).

Our result for  $\alpha_{R,c}$  at  $\gamma = -0.2$  is consistent with those obtained for other actions [15] and thus further supports the conjectured universality of  $\alpha_{R,c}$  in the pure U(1) gauge theory.

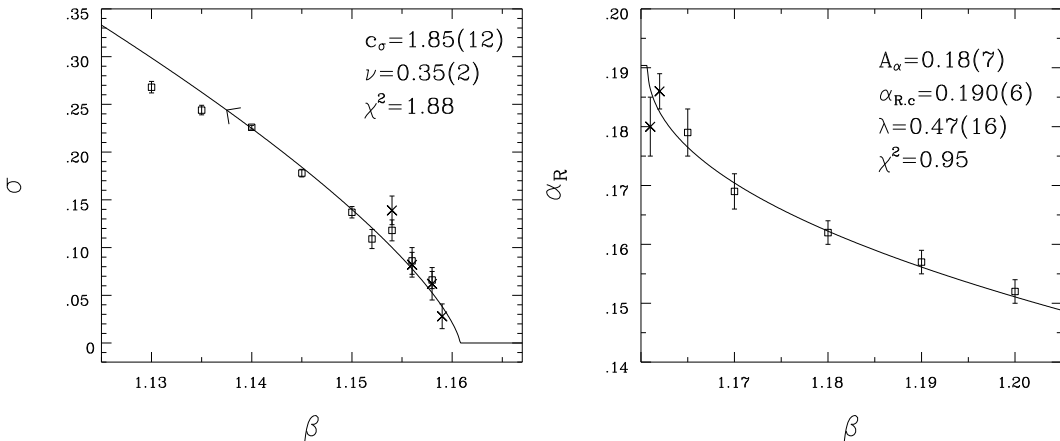


Fig. 1. (a)  $\sigma$  in the confinement phase. The line is the fit (8) of data at  $\beta \geq 1.140$ . (b)  $\alpha_R$  in the Coulomb phase. The line is the fit (11). The lattice sizes are  $16^3 32$  (squares) and  $20^3 40$  (crosses).

## 4 The gauge-ball measurements

### 4.1 Quantum numbers

Our GB operators for a given time-slice are composed of appropriately symmetrized loops containing links only in the three spatial directions. The combinations of loops must have a well-defined behaviour under the point group for cubic symmetry with inversion,  $O_h$ . For rotations one has the proper cubic group  $O$  with its five irreducible representations  $R = A_1, A_2, E, T_1$  and  $T_2$  of dimensions 1, 1, 2, 3 and 3 respectively. Inversion then introduces the parity quantum number  $P = \pm 1$ , involving direct group product such that  $O_h$  behaves as  $O \otimes P$ .

As the representations are complex, we can take the real or imaginary part of the loop, corresponding to charge parity  $C = +1$  and  $-1$ , respectively.

irr. rep.	dimension	smallest spins
$A_1$	1	0, 4, ...
$A_2$	1	3, 6, ...
$E$	2	2, 4, ...
$T_1$	3	1, 3, ...
$T_2$	3	2, 3, ...

Table 4

The smallest spins that are contained in the irreducible representations of the cubic group [30].


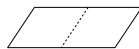

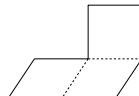
type	# links	# orientations	shape
plaquette	4	3	
rectangle	6	6	
chair	6	12	
flange	8	48	

Table 5

Loops used for the construction of the gauge-ball operators. Their shapes are extended only in the spatial directions.

Thus a complete categorization of a state is  $R^{PC}$  with the five possible  $R$  as above [30].

In the following we consider all these 20 states with momentum  $p = 0$  as well as some with  $p = 1$  (in units of  $2\pi/L_s$ ). We denote these channels by

$$j = R^{PC}(p). \quad (13)$$

The representations  $R$  contribute in the continuum limit to spin as indicated in table 4. In glue-ball calculations one tends to identify the lowest energy lattice state with the lowest continuum spin to which it contributes, but this is not necessarily correct.

For  $p = 1$ , the states no longer have exactly the symmetry of  $O_h$  representations as there is no longer a definite parity. Thus in general our non-zero momentum states have been chosen to minimize the problem of mixing between states. In most channels the  $p = 1$  results simply confirm those for

$p = 0$ . In these cases either the mixing is negligible or the mixed states have higher masses than the ground state of the ‘native’ channel. Two exceptions in the confinement phase and one (the photon) in the Coulomb phase are noted in our discussion of the results.

We have used the loops shown in table 5. In particular the eight-link operator (flange) has no remaining symmetry and so contributes to all  $J^{PC}$ . One can calculate how the various loop orientations project onto states of  $O_h$  using the tables in [30,31]. Thus for zero momentum states we have used suitable combinations of loops to represent the representations of  $O_h$  and determined the lowest lying states in all channels. In order to identify the massless photon in the Coulomb phase we have to use a non-zero momentum. We discuss this further below.

#### 4.2 Improved operators and effective energies

To improve the operators we have used the standard factor-of-two blocking prescription [27]. Accordingly, sets of links on the original lattice are combined together to form links of twice the length by adding the contributions from the central link of length  $2a$  plus all four spatial ‘‘staples’’ of length  $4a$ :

$$\begin{aligned}
U^{(1)}(x, \mu) = & U(x, \mu)U(x + \hat{\mu}, \mu) \\
& + \sum_{\text{spatial } \nu \neq \mu} \left[ U(x, \nu)U(x + \hat{\nu}, \mu)U(x + \hat{\nu} + \hat{\mu}, \mu)U^\dagger(x + 2\mu, \nu) \right. \\
& \left. + U^\dagger(x - \hat{\nu}, \nu)U(x - \hat{\nu}, \mu)U(x - \hat{\nu} + \hat{\mu}, \mu)U(x - \hat{\nu} + 2\hat{\mu}, \nu) \right]. \quad (14)
\end{aligned}$$

The resulting complex number is normalized back to an element of  $U(1)$  with unit modulus. This operation is essentially a block-spin renormalization transformation to a coarser lattice and can be performed recursively, generating  $U^{(2)}$  from  $U^{(1)}$  and so on. The practical limit is reached when the Wilson loop combinations constructed from these blocked links reach the size of the spatial lattice.

This gives us many operators  $O_j^r(t)$  for a GB state  $j$  at Euclidean time  $t$ , where the index  $r$  now labels all contributions from different blocking levels and loop shapes to a given  $j$ . From this one can form a connected hermitean correlation matrix,

$$C_j^{rs}(t) = \sum_{t_0} [\langle O_j^{r*}(t_0 + t)O_j^s(t_0) \rangle - \langle O_j^{r*}(t_0 + t) \rangle \langle O_j^s(t_0) \rangle]. \quad (15)$$

The correlation matrix (at least for a complete set of states) allows for a

spectral decomposition

$$C_j^{rs}(t) = \sum_k A_j^{rsk} \left( e^{-E_j^k t} + e^{-E_j^k(L-t)} \right), \quad (16)$$

where we assume nondegenerate eigenvalues. The coefficients  $A_j^{rsk}$  represent the projections of our GB operators on the energy eigenstates. Since we have only a limited number of states we have to assume that the diagonalization of the truncated matrix still gives the physical energies to a good approximation. The dominant contribution to the matrix at large  $t$  comes from low mass states, which are the ones we are most interested in.

We now diagonalize the correlation matrix by analogy with [28,32,33]. The actual operation we perform can be written as a generalized eigenvalue problem,

$$C_j(t_0 + 1)v_j = \lambda_j C_j(t_0)v_j \quad (17)$$

in which we pick the eigenvector  $v_j$  corresponding to the smallest energy, and hence the largest eigenvalue  $\lambda_j$  (the  $rs$  indices have been suppressed). Solving this is simplified by the fact that the  $C_j(t)$  have all been symmetrized. The larger we choose  $t_0$  here, the smaller the contribution from higher states. However, the statistical fluctuations increase rapidly with  $t_0$  and in practice the gain in stability by picking  $t_0 = 0$  is more important when looking only at the lowest few states. The corresponding  $v_j$  determines the linear combination of operators used for all subsequent analysis at every  $t$ . Its correlator  $c_j(t)$  gives the effective energy and the full correlation matrix is not required again.

Another practical point is that many of the contributions to  $C_j$  actually have very similar sets of coefficients  $A_j^{rsk}$  for these lowest states, making the diagonalization less stable. It should be remembered that the index  $j$  labels blocking level as well as the Wilson loop shape: we have reduced the number of operators which appear in the correlation matrix by picking out the loop shape with the smallest  $\epsilon_j(0) = \log(C_j^{rr}(0)/C_j^{rr}(1))$  from each blocking level, and simply discarding the rest. Thus between 3 and 5 states actually remain in the correlation matrix, depending on the lattice size. The effect of the blocking — the projection onto the lowest state increases ( $\epsilon_j(0)$  decreases) and then falls off again as the amount of blocking is increased — means that this provides a good spread of  $A_j^{rsk}$  and the diagonalization in all cases works well. Where a comparison is possible the results for the lowest mass are indistinguishable from those with the full correlation matrix. We have found that the blocking and diagonalization of the correlation matrix works essentially as well as has been found in pure gauge QCD [28].

The effective energies  $\epsilon_j(t)$  are obtained from the correlation  $c_j(t)$  by solving



numerically the following two coupled equations for  $\epsilon_j(t)$  and  $K_j(t)$ ,

$$\begin{aligned} c_j(t) &= K_j(t)(e^{-\epsilon_j(t)t} + e^{-\epsilon_j(t)(L_t-t)}), \\ c_j(t+1) &= K_j(t)(e^{-\epsilon_j(t)(t+1)} + e^{-\epsilon_j(t)(L_t-t-1)}). \end{aligned} \quad (18)$$

Their approximate solution for small  $t$  is

$$\epsilon_j(t) = \log \frac{c_j(t)}{c_j(t+1)}. \quad (19)$$

### 4.3 Errors of effective energies

The errors of the effective energies  $\epsilon_j(t)$  were obtained directly by the bootstrap method. In this procedure, data consisting of  $N_d$  sets is sampled to produce a new ensemble of  $N_d$  sets; each sample is completely random, so that the new ensemble can contain any of the original sets more than once or not at all. This ensemble is then processed in exactly the same way as the original. The procedure is then repeated an arbitrary but suitably large number of times  $N_{bs}$ , producing a spread of  $N_{bs}$  results. The standard deviation of these results gives a reliable estimate of the statistical error in the original ensemble.

Our initial data was blocked down by a factor 50, producing an  $N_d$  of typically a few tens of data sets for each observable. We have picked  $N_{bs} = 99$ . We have checked that using the same variational basis for all the bootstrap data, rather than re-diagonalizing the correlation matrix for each bootstrap sample, does not affect the errors obtained, and have therefore performed the bootstrap on the data only after the diagonalization.

We have arbitrarily chosen only to look at the first eight correlations and hence seven  $\epsilon_j(t)$  for  $t = 0$  to 6. The choice of the range of  $t$  over which we perform fits to extract the real energies  $E_j$  is described in the next section.

We have analyzed the appropriate range of effective energies in two ways: firstly, using a one-parameter uncorrelated fit to the data over the chosen range of  $t$ , and secondly by taking a weighted mean of all the values over the range. Using the second method we processed the bootstrap samples with the same weights, giving an estimate of the overall statistical error which is presumably more reliable than that on the fit parameter. Certainly the errors with this method appear consistently larger than with the other; some effective energies have an error larger by a factor of around two. This is particularly noticeable in the states near to the phase transition with a good signal. We have therefore used the values from the bootstrap of the weighted means for

our statistical errors.

This analysis gives essentially statistical errors only. An estimate of the systematic errors of our final results will be made at the end of the next section.

## 5 Scaling of the GB masses in the confinement phase

### 5.1 Gauge-ball energies and masses

The list of GB channels we have investigated is given in the first column of table 6. The momenta considered are indicated in parentheses. In the second column we give the quantum numbers of the expected continuum state with the smallest spin, in accordance with the table 4.

In two cases our results for the confined phase should be interpreted as showing a clear signal for mixing when the momentum is non-zero, and hence the naive  $J^{PC}$  interpretation is not correct. These states, the  $T_1^{-+}$  and  $T_2^{--}$ , are marked with an asterisk in table 6. For  $p = 0$  they give no clear signal, increasing the likelihood that states mixed from other  $J^{PC}$  will be visible. To see that the mixing is as expected, one needs to consider the behaviour of  $O_h$  states when the symmetry is broken along a particular axis, as by our  $(1, 0, 0) \times 2\pi/L_s$  momentum boost. The reduced symmetry group is dihedral: one finds that the  $T_1^{-+}$  component whose own axis of symmetry lies along the momentum axis (i.e. longitudinally polarized) has the same behaviour under the reduced symmetry group as the  $A_1^{++}$ , and that the  $T_2^{--}$  likewise mixes with the  $T_2^{+-}$ . This agrees with our results. Also the channel  $T_2^{-+}(1)$  might have an admixture from one of the  $2^{++}$  states (see below).

In each channel we have determined the effective energies  $\epsilon_j(t)$  for as many  $t \leq 6$  as possible. In principle one should obtain each GB energy  $E_j$  by a fit to their plateau which is expected at large  $t$ . In practice, in some channels plateaus can be found only at moderate  $t$ , since  $\epsilon_j(t)$  has very large errors or is unmeasurable for larger  $t$ . The quality of the plateaus is therefore different in different channels and varies with  $\beta$ , being best close to  $\beta_c$ . Sometimes we cannot identify a plateau at all.

We therefore classify the channels according to the quality of the signal for a definite GB energy  $E_j$ , and extract this energy in somewhat different ways. The classification is indicated in the third column of table 6; this holds only for the confinement phase. The meaning is as follows:

**+++ states:** At most  $\beta$  a plateau in  $\epsilon_j(t)$  was found and fitted at  $t \geq 2$ .

Table 6

GB states with momentum  $p = 0, 1$  (in the units  $L_s/2\pi$ ) observed in various channels in the confinement phase and their scaling behaviour. If two momenta are listed in one line, the mass has been assumed to be the same. The quantum numbers of the continuum states with smallest possible spin are indicated in the column “continuum”. The clarity of the effective energy plateau and the reliability of the mass determination is indicated by a corresponding number of “+”. In the channels denoted “?” the evidence for a mass is not clear. In the columns “ $\nu$ ” and “mass” the scaling exponent of the GB mass and its approximate proportionality to one of the mass scales is indicated. The ratio of each mass to the corresponding mass scale is given in the column “ratio”. For the explanation of the continuum states marked with \* see the text.

$R^{PC}(p)$	continuum	quality	$\nu$	mass	ratio		
$A_1^{++}(0, 1)$	$0^{++}$		$\nu_g$	$m_g$	1		
$T_1^{-+}(1) *$	$0^{++} *$				1.01(6)		
$A_2^{+-}(0)$	$3^{+-}$	+++	$\nu_{ng}$	$m_{ng}$	1.00(4)		
$E^{+-}(0)$	$2^{+-}$				0.98(4)		
$T_1^{+-}(0, 1)$	$1^{+-}$				1		
$T_2^{+-}(0, 1)$	$2^{+-}$				1.00(4)		
$T_2^{--}(1) *$	$2^{+-} *$				1.04(5)		
$E^{++}(0, 1)$	$2^{++}$	++		$\nu_{ng}$	$\simeq 2m_{ng}$	2.06(9)	
$T_2^{++}(0, 1)$	$2^{++}$					2.07(9)	
$A_1^{-+}(0)$	$0^{-+}$	+			$\nu_{ng}$	$(2.6 - 3.6)m_{ng}$	2.88(13)
$A_1^{--}(0)$	$0^{--}$						2.73(14)
$A_2^{++}(0)$	$3^{++}$						3.22(16)
$A_2^{--}(0)$	$3^{--}$		2.73(15)				
$E^{--}(0)$	$2^{--}$		2.95(14)				
$T_1^{++}(0, 1)$	$1^{++}$		3.61(18)				
$T_1^{--}(0, 1)$	$1^{--}$		2.94(13)				
$T_2^{-+}(0)$	$2^{-+}$		3.10(14)				
$T_2^{-+}(1) *$	$2^{++} *$		2.63(12)				
$T_2^{--}(0)$	$2^{--}$		3.25(16)				
$\sqrt{\sigma}$				$1/3m_{ng}$	0.34(2)		
$A_1^{+-}(0)$	$0^{+-}$	?		?			
$A_2^{-+}(0)$	$3^{-+}$						
$E^{-+}(0)$	$2^{-+}$						
$T_1^{-+}(0)$	$1^{-+}$						

- ++ **states:** At most  $\beta$  a plateau in  $\epsilon_j(t)$  was found only if  $t = 1$  was included. This plateau was then fitted.
- + **states:** A plateau in  $\epsilon_j(t)$  was found only at the highest statistics point  $\beta = 1.159$  if  $t = 1$  was included. This plateau was then fitted. For other  $\beta$  the value of  $\epsilon_j(1)$  was taken for the GB energy  $E_j$ .
- ? **states:** No plateau in  $\epsilon_j(t)$  was found at  $t \geq 1$  even for  $\beta = 1.159$ . Then we do not obtain any GB energy.

In order to illustrate the quality of the data, we show in fig. 2a results for the effective energies of  $A_1^{++}$  (+++ quality) and  $T_2^{++}$  (++ quality) with  $p = 0$  obtained at a typical data point  $\beta = 1.145$  on the  $16^3 32$  lattice. The effective energies of the same states at the data point with best statistics and smallest errors,  $\beta = 1.159$  (close to  $\beta_c$ ) on the  $20^3 40$  lattice, are shown in fig. 2b. The GB energies  $E_j$  with errors are shown as horizontal lines.

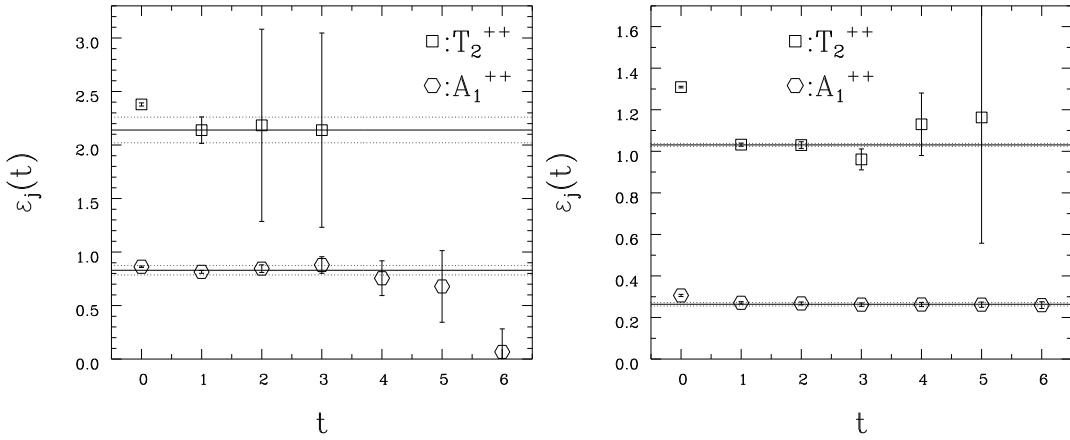


Fig. 2. Effective energies from  $A_1^{++}(0)$  and  $T_2^{++}(0)$  correlation functions (a) at  $\beta = 1.145$  on the  $16^3 32$  lattice and (b) at  $\beta = 1.159$  on the  $20^3 40$  lattice. The plateaus were fitted omitting the points at  $t = 0, 1$  for  $A_1^{++}$  and the point  $t = 0$  for  $T_2^{++}$ . The GB energies  $E_j$  and their errors are indicated by the horizontal lines.

The GB energies  $E_j$  at  $p = 0$  and  $p = 1$  have been used to calculate the GB masses  $m_j$  by the lattice dispersion relation

$$2(\cosh E_j - 1) = m_j^2 + 2 \sum_{\mu=1}^3 (1 - \cos p_\mu). \quad (20)$$

If the masses found in the  $p = 0$  and  $p = 1$  channels with the same  $R^{PC}$  turned out to be consistent, we have continued the analysis assuming their equality, i.e. they were fitted by exactly the same parameters. In the table 6 these “pair” channels are represented by one line only, as well as by the same symbol in the figures 3 and 6.

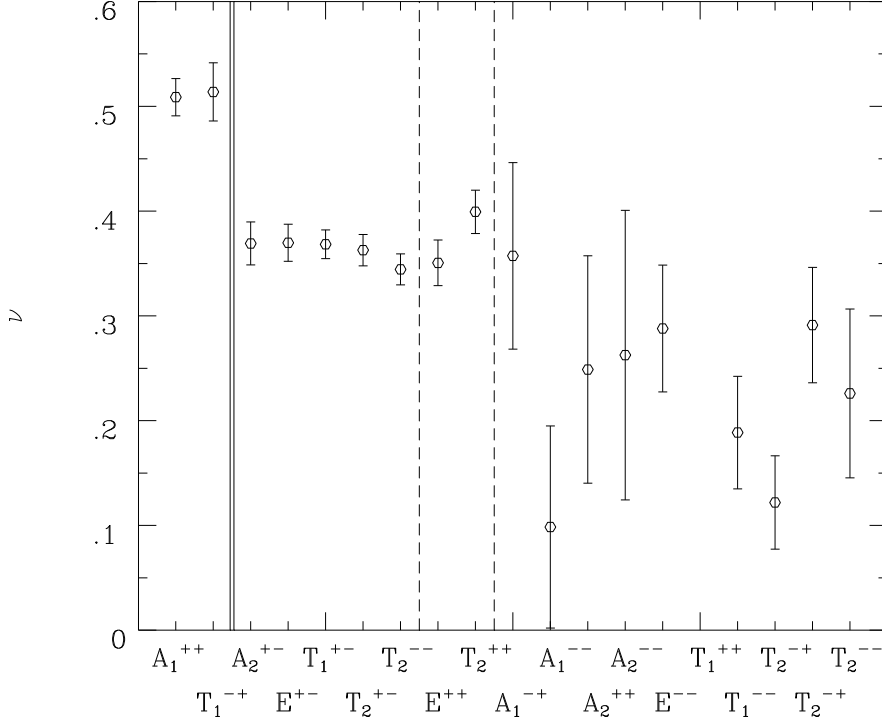


Fig. 3. Values of  $\nu_j$  obtained in each channel separately. The double vertical line separates two groups with distinctly different  $\nu_j$ . The dashed vertical lines separate channels with different quality signal within the group with non-Gaussian exponent values. The ordering within this group is with decreasing reliability (table 6) from left to right.

## 5.2 Two mass scales

Having determined the GB masses for various  $\beta$  we have investigated their scaling behaviour with  $\beta$ . First the fits of the form

$$m_j = c_j(\beta_c^j - \beta)^{\nu_j} \quad (21)$$

were performed for each GB channel  $j$  individually. We found two groups of masses with strikingly different scaling behaviour. Within the whole  $\beta$  range a large group of the GB masses scales with roughly the same exponents  $\nu_j$  close to the non-Gaussian value 0.365(8) found in [8–10]. However, in a small group consisting only of the  $A_1^{++}$ ,  $p = 0, 1$  and the  $T_1^{-+}$ ,  $p = 1$  channels the values of  $\nu_j$  are approximately Gaussian, i.e. 1/2. The values  $\beta_c^j$  are quite consistent with each other in all channels. Therefore, in the further analysis we have assumed the same value of  $\beta_c$  in all channels.

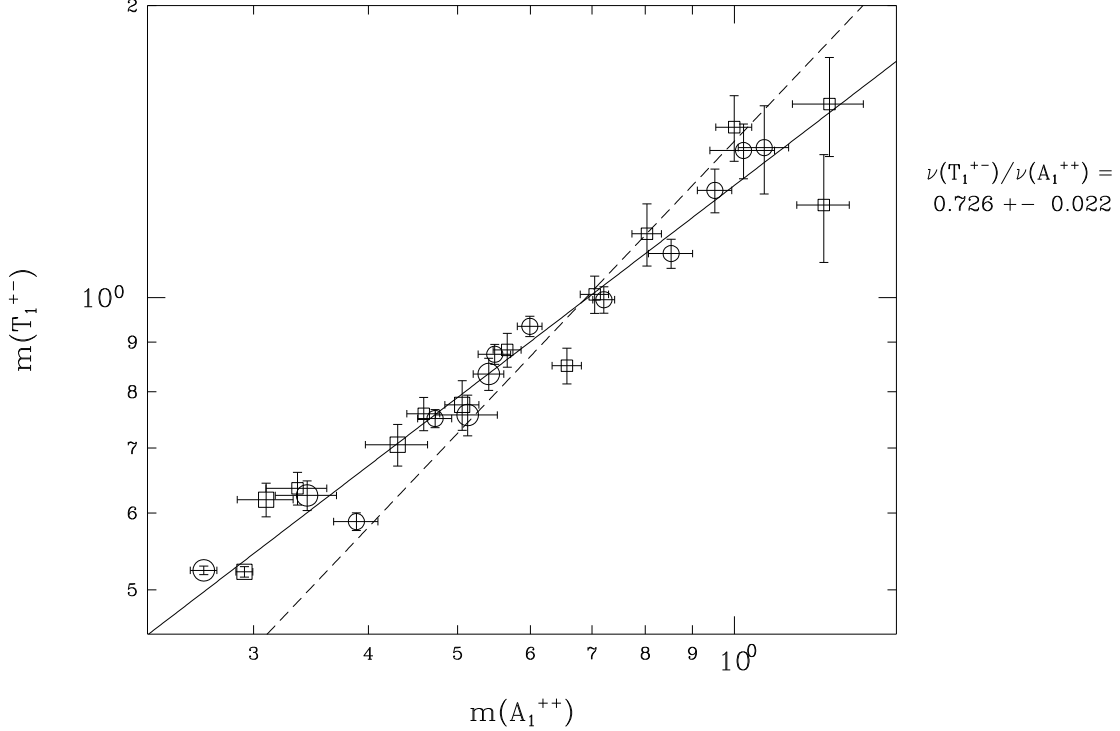


Fig. 4. A log-log plot of the masses of the  $A_1^{++}$  and  $T_1^{+-}$  gauge-balls in the interval  $1.13 \leq \beta \leq 1.159$ . The results from the channels with  $p = 0, 1$  are denoted by circles and squares, respectively. The solid line is the result of a straight line fit considering errors in both directions. The dashed straight line with a gradient of one, i.e. assuming equal exponents, is shown for comparison.

The results for  $\nu_j$  obtained from (21) with common  $\beta_c$  are shown in fig. 3. A clustering around two values is clearly seen. In order to further demonstrate the difference of the scaling behaviour between the two groups we plot the masses of the clearest members of each group, the  $T_1^{+-}$  and  $A_1^{++}$  channels with  $p = 0, 1$ , in a log-log plot against each other in fig. 4. The data have a slope distinctly different from one.

Naturally, as seen in fig. 3, the errors of  $\nu_j$  in channels with less accurately determined masses are rather large. However, for example in the  $T_1^{+-}$  and  $A_1^{++}$  channels with  $p = 0$  and  $p = 1$  the masses are quite accurate and the statistical errors are small. Performing fits to each of these two channels with both momenta we obtain

$$\begin{aligned} \nu_{(T_1^{+-}, p=0,1)} &= 0.37(3), \\ \nu_{(A_1^{++}, p=0,1)} &= 0.51(3). \end{aligned} \tag{22}$$

The masses in these two channels with both momenta (distinguished by different symbols) are shown in fig. 5. The corresponding fits by means of (21)

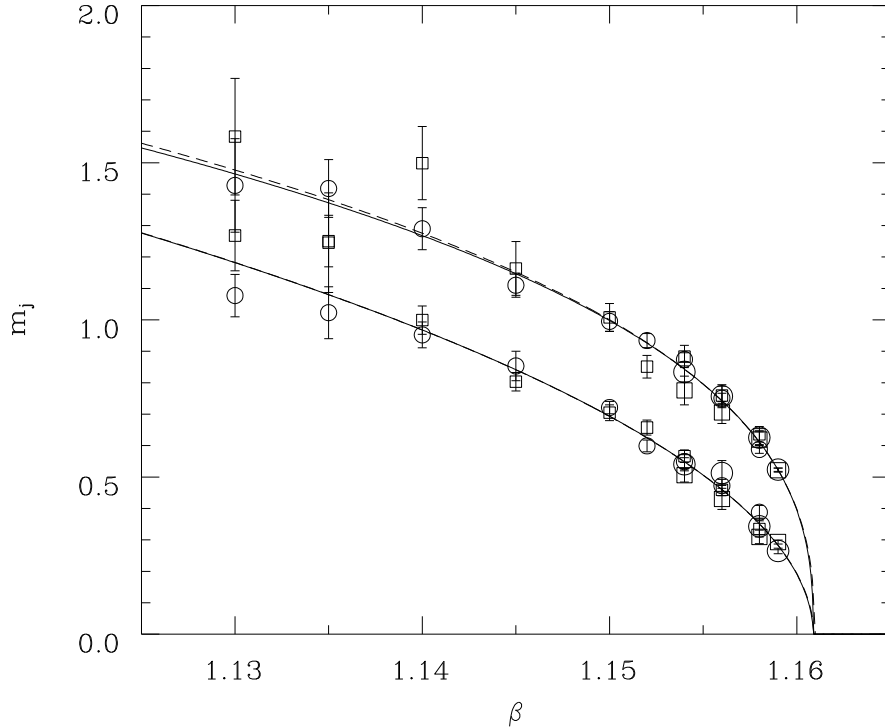


Fig. 5. Masses of the  $A_1^{++}$  (lower points) and  $T_1^{+-}$  glueballs in the confinement phase versus  $\beta$  for both momenta ( $p = 0, 1$  being denoted by circles and squares, respectively). The dashed curves are fits to the data shown. The full curves represent the mass scales (26).

are indicated by dashed lines.

These observations suggested the next step of the analysis: we have assumed the same exponent  $\nu_j$  for each group, denoted  $\nu_{\text{ng}}$  and  $\nu_{\text{g}}$  for the non-Gaussian and Gaussian group, respectively. Then a joint fit was performed with these two exponents, common  $\beta_c$ , and the individual amplitudes  $c_j$  as free parameters:

$$m_j = c_j \tau^{\nu_f}, \quad f = \text{ng, g.} \quad (23)$$

The resulting values of the exponents are

$$\begin{aligned} \nu_{\text{ng}} &= 0.367(14), \\ \nu_{\text{g}} &= 0.51(3). \end{aligned} \quad (24)$$

They are essentially determined by the most accurately determined masses, such as those in the  $T_1^{+-}(0, 1)$  and  $A_1^{++}(0, 1)$  channels. The critical point at

$\gamma = -0.2$  determined in this way is

$$\beta_c = 1.1609(2). \quad (25)$$

The amplitudes, giving the ratios of the masses in each group, are described below.

All the reliably determined GB masses are well described by this fit. Those which are not fully reliable are at least consistent with it. From this we conclude that the system has two mass scales which we denote by  $m_{\text{ng}}$  and  $m_{\text{g}}$ . Each GB mass scales according to one of these mass scales. We choose the fitted scaling behaviour of the GB operators  $T_1^{+-}$  and  $A_1^{++}$  to define the two mass scales:

$$\begin{aligned} m_{\text{ng}} &= c_{\text{ng}} \tau^{\nu_{\text{ng}}}, & c_{\text{ng}} &= c_{(T_1^{+-}, p=0,1)} = 5.4(3), \\ m_{\text{g}} &= c_{\text{g}} \tau^{\nu_{\text{g}}}, & c_{\text{g}} &= c_{(A_1^{++}, p=0,1)} = 7.4(6). \end{aligned} \quad (26)$$

The full curves in fig. 5 represent these mass scales  $m_{\text{ng}}$  and  $m_{\text{g}}$ . We observe that the dashed curves are almost indistinguishable from the mass scales (26). Our determination of these scales is thus not sensitive to the selection of only one channel (with both  $p$ ) data for their definition, nor to the use of a joint value for  $\beta_c$ .

### 5.3 Gauge-ball spectrum

Table 6 summarizes the results for the GB masses in the confinement phase and gives the observed masses in multiples of the two “standard” masses  $m_{\text{ng}}$  and  $m_{\text{g}}$ . For the states denoted by + our assignment is only tentative.

The results for the individual masses are presented in fig. 6 and in the last two columns of table 6. In fig. 6 the individual amplitudes  $c_j$  are shown. They summarize our results for the masses obtained from all  $\beta$  points in the confinement phase and reflect their scaling behaviour. It is apparent that the states in the non-Gaussian group cluster around three values of  $c_j$ , being multiples of the lowest mass states in this group.

An alternative way to determine the GB masses is to rely only on the high statistics data point,  $\beta = 1.159$  on the  $20^3 40$  lattice. The absolute values of  $m_j$  at this point are presented in fig. 7. Here we show the results for  $p = 0$  and  $p = 1$  separately in all channels, including the pairs. Of course, at one fixed  $\beta$  the difference in the scaling behaviour is not observable. However, keeping in mind that there are two groups of states, one can compare figs. 6 and 7 for



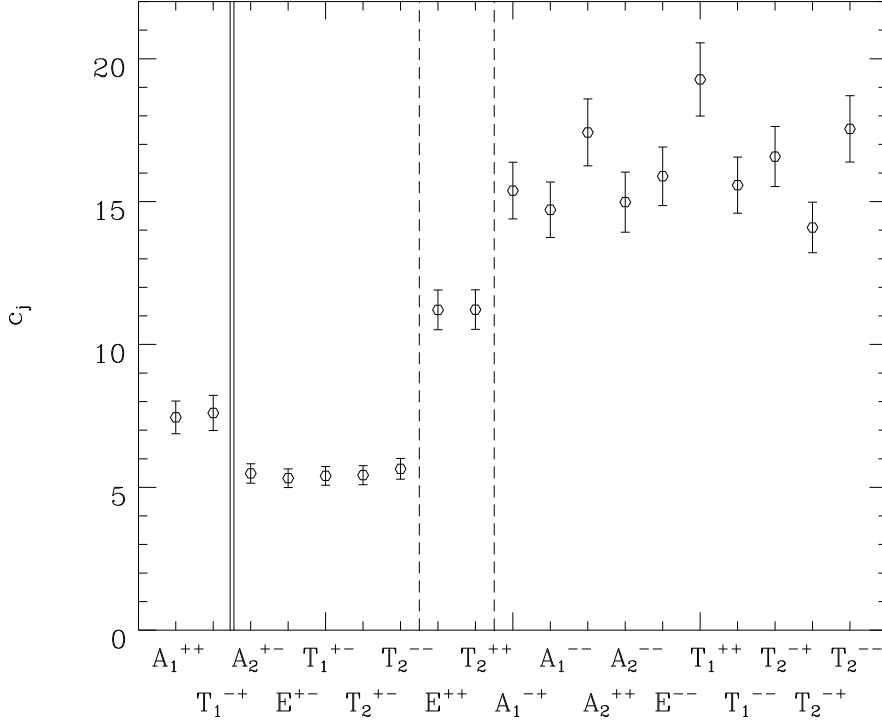


Fig. 6. The amplitudes  $c_j$  of the fits (23). The vertical lines have the same meaning as in fig. 3.

each group separately and find an agreement between the mass ratios. The two-fold and perhaps three-fold clustering of the values in the non-Gaussian group around the lowest mass is again apparent.

As seen in fig. 7, the dispersion relation (20) is slightly violated for the pairs  $E^{++}(0, 1)$  and  $T_2^{++}(0, 1)$ . Motivated by the fact that the corresponding masses are very close to  $2m_{\text{ng}}$ , we have also tried to apply the dispersion relation assuming that it is really two-particle states which are seen in these channels, either both particles having zero momentum or one of the particles moving with the lowest nonzero momentum. Indeed, the fit of  $E_j$  in these channels gave the mass  $m_{\text{ng}}$  for each of the two particles even for  $p = 1$ . This result is indicated by crosses in fig. 7. It suggests that the  $E^{++}(0, 1)$  and  $T_2^{++}(0, 1)$  channels are dominated by states of two gauge-balls from the non-Gaussian group with mass  $m_{\text{ng}}$ . Of course, further verification of such a possibility is necessary.

Only the ratios of the amplitudes within each group are relevant for the continuum limit, and therefore we show in the last column of table 6 the ratios  $r_j$  to the corresponding mass scales (26),

$$m_j = r_j m_f, \quad f = \text{ng, g.} \quad (27)$$

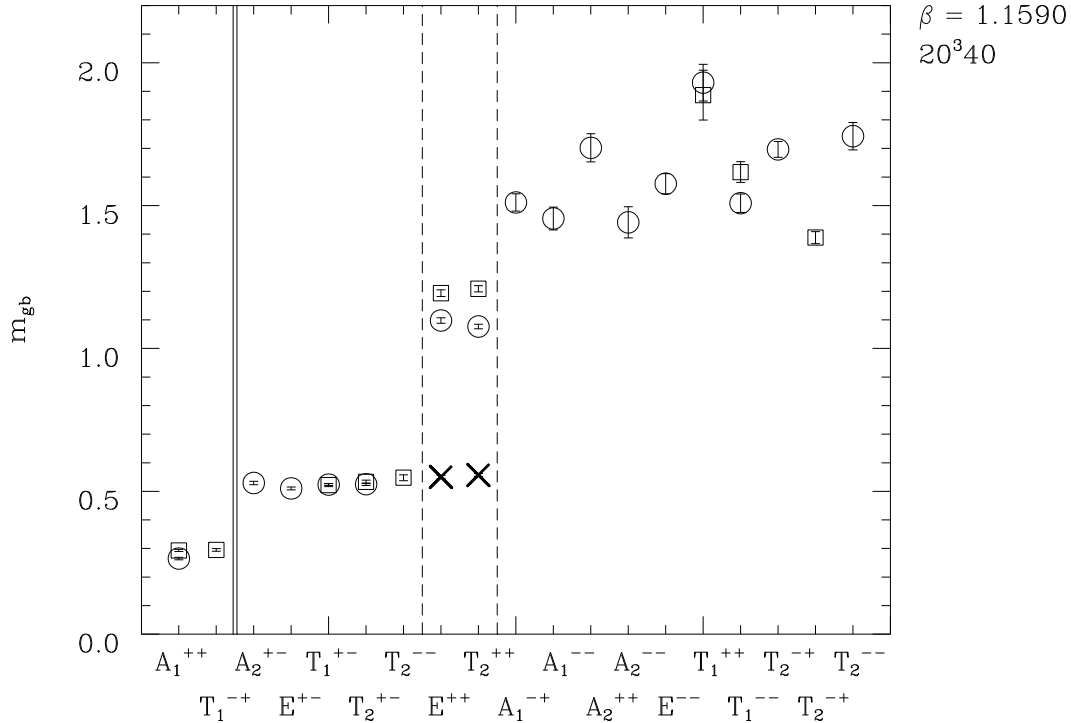


Fig. 7. GB masses  $m_j$  at the point with the highest statistics,  $\beta = 1.159$  on the  $20^3 40$  lattice. The  $p = 0, 1$  results are indicated by the circles and squares, respectively. The crosses belonging to the  $E^{++}(0, 1)$  and  $T_2^{++}(0, 1)$  channels are masses of individual particles when the energies  $E_j$  in these channels with  $p = 1$  are assumed to correspond to two-particle states with lowest nonzero momentum. The vertical lines have the same meaning as in fig. 3.

Relating the different scales set by the string tension and by the mass  $m_{ng}$

$$\sqrt{\sigma} = r_\sigma m_{ng}, \quad (28)$$

we obtain

$$r_\sigma = 0.34(2). \quad (29)$$

This value is given in table 6 for a comparison with the GB masses.

It is interesting to compare our results in the confined phase with those of quenched QCD (i.e. pure gauge  $SU(3)$ ), for which the most recent analysis of all  $J^{PC}$  appeared in ref. [34] (see in particular fig. 1), and of the  $A_1^{++}$  and  $E^{++}$  also in [35]. Although our results here are spread over a larger variety of lattice sizes and couplings, the higher efficiency of  $U(1)$  calculations implies that the statistical accuracy of the results is comparable in the two cases.

As in SU(3), we find that masses tend to appear together in bands. This is more pronounced in our case as it appears in low-lying and therefore well measured states. In both cases we find the lowest lying state to be the most symmetric, namely  $0^{++}$ . We also find a low-lying  $2^{++}$  (lattice  $E^{++}$  and  $T_2^{++}$ ) state. A clear difference to SU(3) is that in the U(1) case there is a band of intervening  $PC = +-$  states for spins 1, 2 and 3, all with similar mass, which do not appear in SU(3) (though in the latter case there is a  $1^{+-}$  state with approximately twice the lowest glueball mass). Indeed, these states in U(1) are the lowest ones with the non-Gaussian scaling behaviour. On the other hand, we do not find the low-lying  $0^{-+}$  (and maybe  $0^{+-}$ , which had a large error) of SU(3).

Heavier states have correspondingly large errors, making any further comparison too difficult. It is at least clear that the similarity of confining behaviour is not by itself enough to guarantee a similar spectrum.

One further similarity to QCD is remarkable: It has been known for long that in the lattice QCD the  $\beta$  dependence of the  $0^{++}$  glueball is somewhat different from that of the other glueball states. We shall return to this point in the next section.

The simplest interpretation of the observed spectrum might be the following: The Gaussian spectrum consist of one scalar  $0^{++}$  only. The non-Gaussian group has a nontrivial but quite simple spectrum consisting of the  $1^{+-}$ ,  $2^{+-}$  and  $3^{+-}$  states of the same mass  $m_{\text{ng}}$ . Higher spin assignments for the  $J^{+-}$  states are not ruled out, however. In the other channels the masses are  $\simeq 2m_{\text{ng}}$  and  $(2.6 - 3.6)m_{\text{ng}}$ . They may well correspond to two- and three-particle states of the lightest non-Gaussian gauge-balls. The multi-particle states of the Gaussian scalar do not seem to contribute significantly to the non-Gaussian channels in spite of its low mass. This further supports the expectation that the  $0^{++}$  belongs to a “trivial” theory.

#### 5.4 Error analysis

The errors given up to now in this section have been obtained by purely statistical procedures. They are based on the essentially statistical errors of the energies  $E_j$  and the corresponding masses  $m_j$ , described in the previous section. As seen in (24) and (25), they are rather low, on the level of 4% for  $\nu_{\text{ng}}$ .

However, it is obvious that various additional errors – partly of systematic origin – should be expected. The main reason is that we have to stay away from the critical point in order to avoid finite size effects and the two-state signal. The value of  $\beta_c$  then enters very sensitively into the determination of

$\nu$  by fits like (23). Furthermore, mass values  $m_j \simeq 1$  have to be used in such a fit. This raises the question of nonleading terms in the scaling behaviour.

To get at least an estimate of these effects, we made several analyses of the scaling behaviour of the well determined (+++) masses when  $\beta_c$  is approached, modifying the procedure in various ways. In most cases the obtained values for  $\nu$  and  $\beta_c$  varied slightly with the procedure.

- (1) We modified the  $\beta$  interval in which the power law fits were performed, dropping up to five  $\beta$  points most distant from  $\beta_c$ . No significant change of the  $\nu$ -values has been observed as long as the same  $\beta_c$  was used.
- (2) Instead of (20) we have used the dispersion relation with  $m_j^2$  replaced by  $2(\cosh m_j - 1)$  (this amounts to  $m_j = E_j$  for  $p = 0$ ). The difference between these two frequently used relations is on the  $O(m^4)$  level and thus indicates a possible effect of nonleading terms.
- (3) We analyzed separately the masses from the  $p = 0$  and  $p = 1$  channels.
- (4) We analyzed separately the masses obtained on the  $16^3 32$  and  $20^3 40$  lattices. This also corresponds to a variation of the  $\beta$  interval close to  $\beta_c$ .
- (5) The same data were fitted both with free  $\beta_c$  and with this value fixed within the interval of its values obtained by other modifications.
- (6) The Gaussian and non-Gaussian group was fitted with independent  $\beta_c$  for each group. The difference of  $\beta_c$  values is about or less than 0.0002.

Dropping the extremal values for each parameter, we found their values lay in the following intervals:  $\nu_{\text{ng}} = 0.32\text{--}0.38$ ,  $\nu_{\text{g}} = 0.41\text{--}0.57$  and  $\beta_c = 1.1605\text{--}1.1609$ . The ratio  $\nu_{\text{ng}}/\nu_{\text{g}} = 0.62\text{--}0.80$  is always clearly different from one. These intervals are significantly broader than the statistical uncertainties. Assuming some peaked distribution of the values in these intervals, we take one quarter of their widths as an estimate of the systematic errors not accounted for by the purely statistical analysis.

The values of the critical exponent  $\nu$  given in (1), (2), (4), and of  $\beta_c$  given in (3) are the central points of these intervals. The quoted errors are the simple sums of the above systematic errors and typical statistical errors.

## 6 Three scenarios

The occurrence of two different correlation length exponents may seem surprising in the light of the simulations on spherical lattices [8–10]; there the scaling of several bulk observables could be well described by means of only one exponent,  $\nu_{\text{ng}}$ . In particular, the Fisher zeros at  $\gamma = -0.2$  showed no deviation from the asymptotic finite size scaling behaviour determined by this value of the exponent  $\nu$ . However, that analysis was based completely on the bulk energy.

In this observable there is little chance of finding nonleading behaviour. The contributions scaling with smaller critical exponents will be dominant near the phase transition. In terms of the eigenvalues  $\lambda_i$  of the linearized renormalization group matrix this is quite understandable: since  $\lambda_i = s^{1/\nu_i}$  (where  $s$  is the scale change factor), the smallest  $\nu_i$  dominates.

Therefore we see no contradiction with the earlier results in the appearance of two different correlation length exponents in our present simulations. Furthermore, it does not appear unnatural when the possibility of the presence of a TCP at  $\gamma = \gamma_0$  is taken into account. The TCP's are known to have exponents in general different from those associated with the adjacent ordinary critical lines [17], and they tend to dominate the scaling behaviour in their vicinity when the critical manifolds are approached from outside. The cross-over regions between tricritical and critical scaling behaviour may extend quite far away at a small angular distance from the critical lines [36,17]. Furthermore, different observables, e.g. correlation lengths, may have different crossover regions.<sup>1</sup>

However, when trying to explain the observed scaling of the GB masses at  $\gamma = -0.2$  with help of the TCP, we see at present no reliable possibility of saying *which one*, if any, of the two observed  $\nu$ -values corresponds to the tricritical scaling. Instead of guessing we formulate three scenarios, which hopefully can be tested in future simulations. In each of them we assume that  $\gamma_0 > -0.2$ .

In all the following scenarios one can consider two different continuum limits, depending on the mass  $m_j^{\text{phys}} = m_j/a$  that one chooses to fix in physical units. If it is one of the non-Gaussian group, then the lattice constant vanishes as

$$a(\tau) = \frac{m_{\text{ng}}}{m_{\text{ng}}^{\text{phys}}} \propto \tau^{\nu_{\text{ng}}}, \quad (30)$$

and analogously for the Gaussian group,

$$a(\tau) = \frac{m_{\text{g}}}{m_{\text{g}}^{\text{phys}}} \propto \tau^{\nu_{\text{g}}}. \quad (31)$$

### Scenario C:

The point  $\gamma = -0.2$  is a critical point with two relevant mass scales, i.e. *both exponents  $\nu_{\text{ng}}$  and  $\nu_{\text{g}}$  are critical*. Two different scaling laws at the same critical point are unusual, but not, to our knowledge, impossible. A somewhat analogous situation is known in the three-dimensional pure compact U(1)

---

<sup>1</sup> We thank D.P. Landau for a helpful advice in this question.

gauge theory [37]. As the ratio of masses approaches zero,

$$\frac{m_g}{m_{\text{ng}}} \propto \tau^{\nu_g - \nu_{\text{ng}}} \propto \tau^{0.5 - 0.365} \rightarrow 0, \quad (32)$$

we can consider two different continuum limits:

- (1) **C<sub>ng</sub>**: Keeping  $m_{\text{ng}}^{\text{phys}}$  constant, the spectrum consists of those GB states which scale with  $\nu_{\text{ng}}$  as states with finite nonzero mass, and the string tension is finite. The  $0^{++}$  GB would be present as a massless state. This would be an interesting continuum theory.
- (2) **C<sub>g</sub>**: Keeping  $m_g^{\text{phys}}$  constant, only the  $0^{++}$  state can have a finite mass, whereas the masses of all other states and the string tension would run to infinity and decouple. Presumably this would be a Gaussian theory with a noninteracting scalar.

This scenario does not make any use of the special properties of a TCP and might hold if there is no TCP with special tricritical exponents at  $\gamma = \gamma_0$ .

In the tricritical scenarios discussed next, we assume the tricritical point at  $\gamma = \gamma_0$  and take into account the possibility that some of our scaling results are not yet asymptotic, but obtained in a domain where a precocious form of scaling with a “wrong” scaling exponent is obtained.

**Scenario T<sub>g</sub>:**

The tricritical point is Gaussian, i.e.  $\nu_g$  is tricritical and  $\nu_{\text{ng}}$  is critical. The continuum limit at  $\gamma = -0.2$  is like that in the scenario **C<sub>ng</sub>** except for the mass of the  $0^{++}$  GB state. That mass shows “wrong” (tricritical, i.e. nonasymptotic at this  $\gamma$ ) scaling behaviour for those distances from  $\beta_c$  we were able to investigate on lattices of limited size. In this scenario it would have to change its scaling behaviour closer to the phase transition, adopting the exponent  $\nu_{\text{ng}}$ . This state could thus have a nonvanishing mass. The data close to  $\beta_c$  suggest that this mass would be small relatively to  $m_{\text{ng}}$ .

At the TCP the continuum limit would be Gaussian and our present results would say nothing about the spectrum there except the presence of the light  $0^{++}$  GB state.

**Scenario T<sub>ng</sub>:**

The tricritical point is non-Gaussian, i.e.  $\nu_{\text{ng}}$  is tricritical and  $\nu_g$  is critical. At  $\gamma = -0.2$  all the GB masses except that of the  $0^{++}$  state, as well as the string tension, show “wrong” (tricritical) scaling behaviour on our lattices but would change to critical scaling when approaching the phase transition more closely. All masses and the string tension stay finite in the continuum limit.

However, because of the Gaussian value  $\nu_g$  the theory might be trivial with logarithmic corrections which we cannot detect.

A nontrivial continuum theory analogous to  $\mathbf{C}_{\text{ng}}$  would then be expected at the TCP. As in  $\mathbf{T}_{\text{ng}}$  at  $\gamma = -0.2$  the  $0^{++}$  state might have a small mass.

At the moment it is difficult to decide which of these scenarios is the correct one, but the most important conclusion holds in any of them: a continuum limit is possible in which the observables scaling like  $m_{\text{ng}}$  remain finite and nonzero in physical units. Their ratios are given by the factors  $r$  in front of  $m_{\text{ng}}$  in eqs. (27) and (28), and in table 6. This nontrivial limit is obtained on the critical line in the scenarios  $\mathbf{C}_{\text{ng}}$  and  $\mathbf{T}_g$ , whereas in the scenario  $\mathbf{T}_{\text{ng}}$  it is obtained at the hypothetical TCP. The ambiguity which remains is the mass in physical units of the  $0^{++}$  GB state in such a continuum limit: it is zero in the  $\mathbf{C}_{\text{ng}}$  scenario whereas in both the  $\mathbf{T}$  scenarios it may be nonzero but small relatively to  $m_{\text{ng}}$ .

Both scenarios  $\mathbf{T}$  imply that in the range of correlation lengths we were able to investigate one of the two groups of channels shows a behaviour at  $\gamma = -0.2$  which actually corresponds to the TCP, and not to the critical point at this  $\gamma$ . This can be explained assuming a broad dominance angle of the TCP for the corresponding states. However, we find it remarkable (peculiar?) that the would-be critical value of  $\beta$  of the group with “false” tricritical behaviour agrees within our precision with that of the other group.

The special behaviour of the  $0^{++}$  (strictly speaking  $A_1^{++}$ ) GB suggests a possible parallel with pure  $SU(N)$  gauge theories with a mixed action. In that case the Wilson action, containing the trace of the plaquette in the fundamental representation, is supplemented by a term where the trace of the plaquette is taken in the adjoint representation with coupling  $\gamma$ . The procedure is analogous to the  $U(1)$  with extended Wilson action. For  $SU(2)$  and  $SU(3)$  the theory has a first order line with an endpoint at positive  $\gamma$ . In the  $SU(3)$  case it was found [38] in this region that, while the  $E^{++}$  mass remains finite, the  $0^{++}$  mass goes to zero. The critical exponent is not known. Other masses have not been calculated, although it is a long-standing result for  $SU(2)$  [39] that the string tension also remains finite around the corresponding end point. Thus the  $0^{++}$  seems to be singled out for special behaviour as it is in the results presented here. In  $SU(3)$  there is presumably no phase transition for values of  $\gamma$  below the endpoint, apart from a near-coincidence with finite temperature effects on small lattices which appears to be accidental [40]<sup>2</sup>. It is therefore natural to suppose the special behaviour is due to the endpoint itself. There

---

<sup>2</sup> The possibility of a different interpretation, very similar to the phase diagram of the  $U(1)$  theory, has been pointed out in [41].

are other examples in lattice models where such endpoints are associated with Gaussian behaviour (see e.g. [42]). Depending on the choice from the above scenarios where the  $0^{++}$  gauge-ball in the U(1) theory scales, either the TCP or the critical line at  $\gamma < \gamma^0$  might be analogous to such endpoints.

## 7 The spectrum in the Coulomb phase

### 7.1 Expected properties of photon and resonance states

In order to prepare the ground for an understanding of our results, let us first discuss the properties of a phase with massless photons and massive GB's on a finite lattice. We will conclude below that this is just what we observe from our data on the GB operator correlation functions.

A massless state projected to zero (spatial) momentum does not decay exponentially. From experience with Goldstone bosons [43] we expect in fact a propagator polynomial (parabolic) in the time variable. However, the operator projected to non-zero momentum will have non-zero energy  $E = |\vec{p}| \propto 1/L_s$  and an  $L_s$ -dependent exponential decay. This explicit finite size dependence is an excellent indicator for massless states. Since states with non-zero momentum are not parity-eigenstates, we expect that in this case the photon continuum state with  $J^{PC} = 1^{--}$  contributes to the  $T_1^{+-}(1)$  channel. Therefore, in the  $T_1^{+-}(0)$  channel there is no signal from the photon, while the  $p = 1$  state has just the energy corresponding to one unit of momentum. Such observations thus demonstrate the presence of a massless photon with continuum quantum numbers  $1^{--}$ .

If, in addition, there is another, now massive, state e.g. in the  $T_1^{+-}$  channel, it will couple to multi-photon states with these quantum numbers and therefore will not be an asymptotic state of the system, but a resonance. The lowest energy state for  $\vec{p} = 0$  is the 3-photon state with photon 3-momenta  $(1,0,0)$ ,  $(0,1,0)$  and  $(-1,-1,0)$  and total energy  $E = (2 + \sqrt{2})$  (again in units of  $2\pi/L_s$ ).

For simplicity of our presentation we use here the continuum dispersion relation, although actually on the lattice (for massless states) we have  $\cosh E = 4 - \sum_{i=1}^3 \cos p_i$ . In the actual analysis and the plots we always use the lattice dispersion relation.

In a finite volume system at fixed value of the coupling we therefore expect a specific behaviour of the (discrete) energy spectrum [44] when  $L_s$  increases. For small  $L_s$  the lowest measured energy will be constant with a value close to the resonance mass and only a weak dependence on  $L_s$ . At some  $L_s$  the lowest



multi-photon state with energy  $\propto 1/L_s$  becomes the lowest energy state. The phenomenon of avoided level crossing will be observed, and the lowest energy will drop inversely proportional to the spatial extension. If one can observe higher levels in the energy spectrum one will see the resonance as the next higher state, until further avoided level crossings with multi-photon states of higher momenta occur. From the energy levels one can (under certain conditions) derive values of the phase shift in the multi-particle channels [44,33,45]

Consider now the variation with the coupling constant. The resonance mass in lattice units then varies with the scale, whereas e.g. the zero-momentum 3-photon energy in lattice units is still  $(2 + \sqrt{2})$ . The avoided level crossing therefore occurs at a different lattice size. This behaviour provides another strong clue for the interpretation of the spectrum.

Finally, for a given lattice size, but as a function of the coupling, the lowest energy level in a resonance channel might increase when moving away from the phase transition; eventually it should approach but never exceed the lowest multi-particle energy level. This level decreases proportional to  $1/L_s$ .

## 7.2 Evidence for resonances

Let us now discuss our results for gauge-balls in the Coulomb phase. Indeed, we find a massless state in the  $\vec{p} = (1, 0, 0)$  channel of  $T_1^{+-}$ , with a size dependence following the expected dispersion relation. We identify this signal with the photon. In the zero momentum channel we find a lowest energy state following the scenario of a resonance coupling to a 3-photon state, as discussed above. For small lattice sizes the lowest energy level is compatible with a constant, until it reaches the 3-photon level, which it follows for larger spatial volumes as seen in fig. 8.

We estimate the position of the resonance from the energy values determined at lattice sizes below the point where the avoided level crossing occurs. We indeed find a consistent behaviour indicating an increase of the correlation length towards the phase transition.

The energy levels in the channel  $A_1^{++}$  exhibit a similar behaviour (fig. 9). This state is also supposedly a resonance, since it couples to a two-photon state (photon three-momenta  $(1,0,0)$  and  $(-1,0,0)$ ) with total energy 2 (in units of  $2\pi/L_s$ ).

In order to provide a further confirmation for the nature of this state we have also determined the second-lowest energy level at  $\beta = 1.17$  and various spatial volumes. As discussed above, we have usually determined the optimal operator from the diagonalization (cf. (17) of the correlation matrix at time

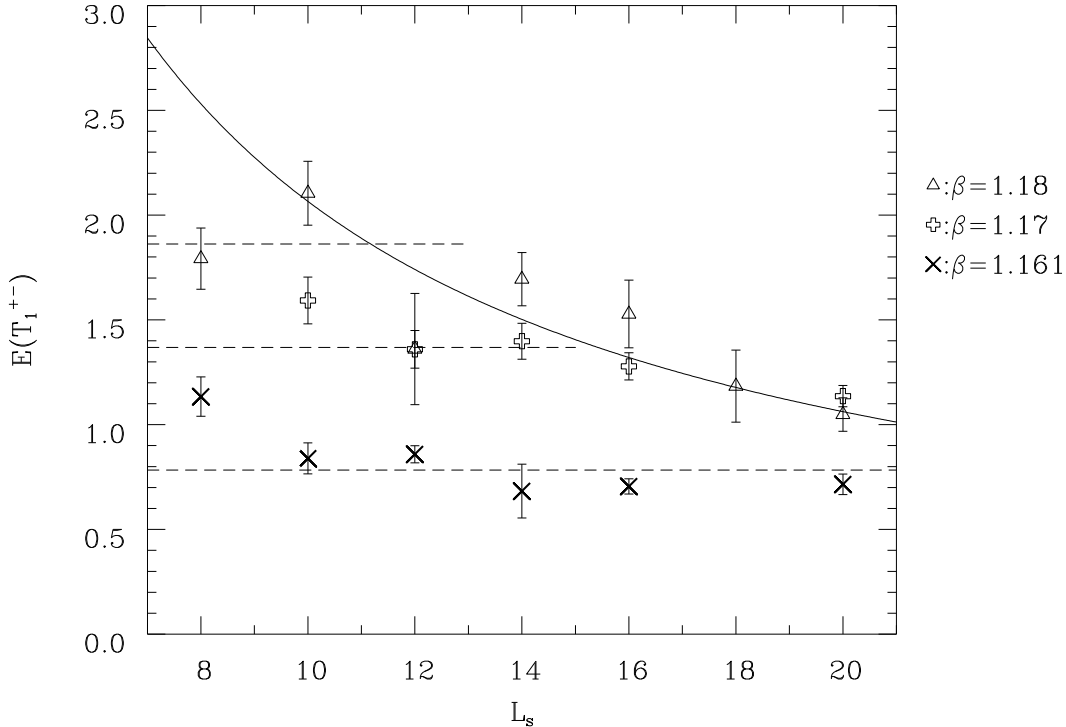


Fig. 8.  $T_1^{+-}(0)$  energy vs.  $L_s$  for  $\beta = 1.18, 1.17, 1.161$  in the Coulomb phase. The full line is the energy of the 3-photon state. The dashed horizontal lines indicate the region of those points that have been included in the mean value for the determination of the resonance positions.

distance  $t_0 + 1 = 1$ . Performing the diagonalization at a larger time might improve results for the excited states. We have tried this, but see no good indication that the effective mass plateau for the higher states is improved, and consequently have used  $t_0 = 0$  again. Fig. 10, albeit with larger errors and uncertainties for the higher lying levels, seems to support our interpretation.

Again we determine the approximate resonance position and we find indication of critical behaviour towards the phase transition. In fig. 11 we give the  $\beta$ -dependence for the masses of  $A_1^{++}$  and  $T_1^{+-}$  states.

The data is not of sufficient quality to decide on the scaling parameters. The determination of masses in the Coulomb phase has various handicaps. On one hand, according to our observations we expect that these states are not asymptotic but resonances. Only a narrow window is used to determine their masses. On the other hand, [25] observed certain effects on the mass measurements of the photon propagator due to the Dirac sheet background and related to gauge fixing [23,24]. We do not expect these to affect our results noticeably since we have comparatively large spatial lattices. Finally, due to the massless state the finite size effects are definitely larger than in the confinement phase.

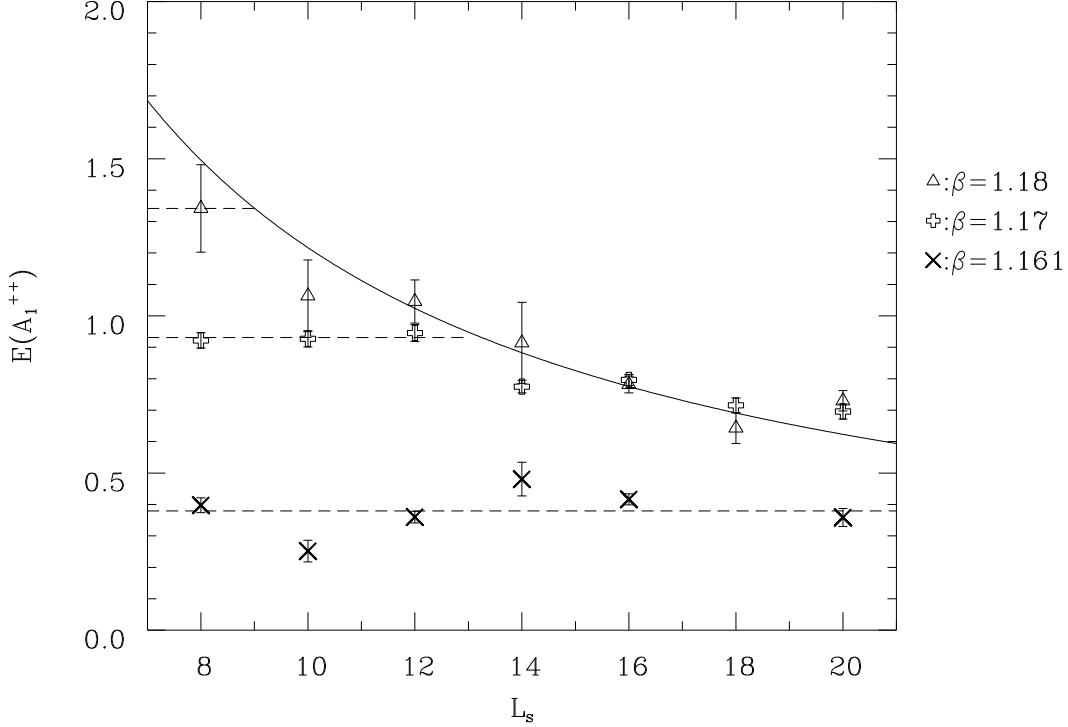


Fig. 9.  $A_1^{++}(0)$  energy vs.  $L_s$  for  $\beta = 1.18, 1.17, 1.161$  in the Coulomb phase. The full line is the 2-photon energy. The dashed horizontal lines indicate the region of those points that have been included in the mean value for the determination of the resonance positions.

We think that this last problem may be the main reason for our difficulties to identify a consistent scaling form from the Coulomb side.

Our results indicate that in the Coulomb phase one has both massless vector states (photons) and massive GB resonances  $A_1^{++}$  and  $T_1^{+-}$  that couple to 2 or 3 of the massless states, respectively. The masses of the resonance states seem to scale towards the phase transition. We cannot decide whether both scale differently or not. However, assuming that the uncertainties associated with the determination of each individual mass partly cancel in their ratio, one can look at whether the log-log plot, analogous to fig. 4 in the confinement phase, has a slope different from one. In fig. 12 we see that the data indeed indicate the slope being consistent with that in fig. 4. This could point towards the existence of two mass scales in the Coulomb phase, too.

As for the other channels, our data suggest that the  $T_2^{+-}(0)$ ,  $A_2^{+-}(0)$  and  $E^{+-}(0)$  behave similar to  $T_1^{+-}(0)$ . Thus massive three-photon resonances, possibly with the same or similar mass, could be present in all these channels. The spectrum of the resonances in the Coulomb phase might thus resemble that of the gauge-balls in the confinement phase.

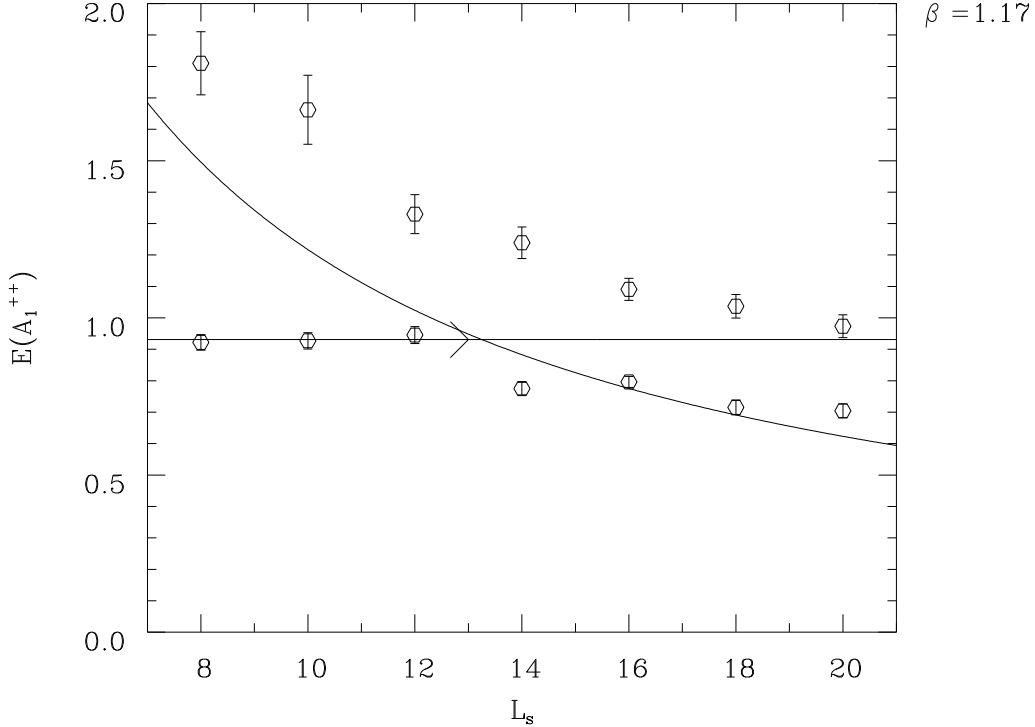


Fig. 10. First two energy levels of the  $A_1^{++}(0)$  energy vs.  $L_s$  for  $\beta=1.17$ . The horizontal line is the fit to the mass on small lattices. The other line represents the lowest two-photon energy.

## 8 Conclusions and open questions

Our results in the confinement phase are in agreement with the earlier finite size studies on spherical lattices [8–10] but substantially extend that work. They strongly suggest the existence of a continuum quantum field theory in four dimensions with the following properties:

- (1) From the confining phase one approaches a non-Gaussian fixed point, so the theory is presumably interacting but not asymptotically free. The correlation length exponent at this fixed point is  $\nu_{\text{ng}} \simeq 0.36$ . This value is obtained by combining our present results with those in [8–10].
- (2) The well measurable physical states at this fixed point contribute to the  $A_2, E, T_1$  and  $T_2$  representations of the lattice symmetry group with  $PC = +-$ . They have equal or very similar mass  $m_{\text{ng}}^{\text{phys}}$ . Assuming that the smallest spin dominates, the continuum quantum numbers of gaugeballs would be  $R^{PC} = 1^{+-}, 2^{+-}, 3^{+-}$ . This assignment is uncertain as it could be that for example the  $3^{+-}$  GB dominates the  $T_1^{+-}$  channel and the  $1^{+-}$  state is not present.
- (3) Depending on the scenario for the continuum limit of the lattice theory,

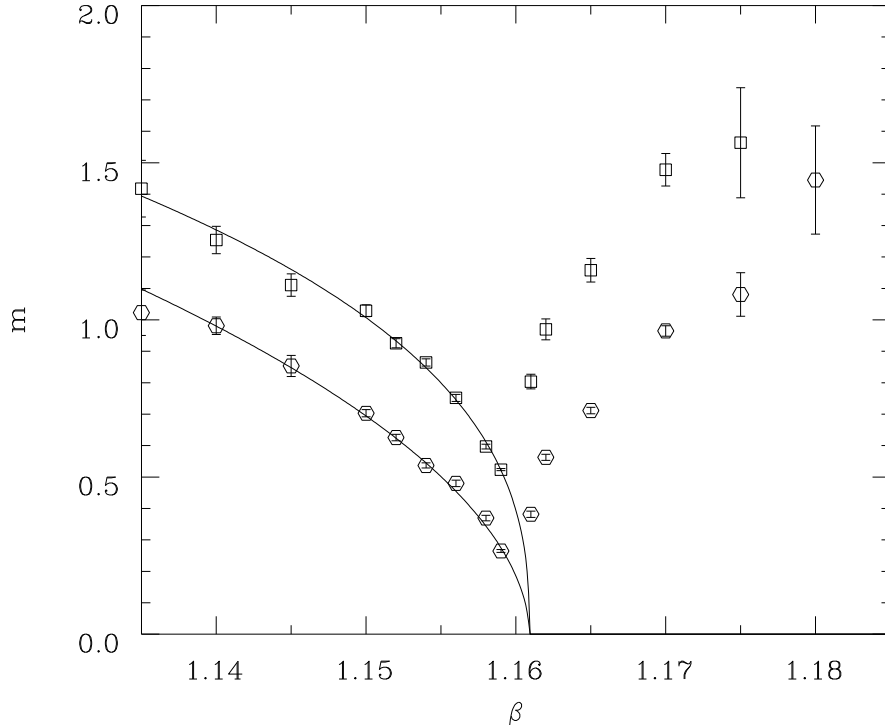


Fig. 11. Resonance masses vs. beta in the Coulomb phase for  $T_1^{+-}(0)$  (squares) and  $A_1^{++}(0)$  (circles). For comparison we show also masses in the same channels in the confinement phase.

the continuum theory might contain a light (compared to  $m_{\text{ng}}^{\text{phys}}$ ), possibly massless  $A_1^{++} = 0^{++}$  gauge-ball. However, it is probably only weakly coupled to the states in other channels, and might be completely decoupled. No other state in the  $A_1^{++}$  channel was observed.

- (4) The theory is confining in the sense of the Wilson criterium, i.e. the string tension in physical units  $\sigma^{\text{phys}}$  has a finite nonvanishing value  $\sqrt{\sigma^{\text{phys}}} \simeq 0.34m_{\text{ng}}^{\text{phys}}$ .
- (5) In the  $E^{++}$  and  $T_2^{++}$  (presumably  $2^{++}$ ) channels a state with  $m_{2^{++}}^{\text{phys}} \simeq 2m_{\text{ng}}^{\text{phys}}$  is present. It may be a two-particle state.
- (6) In many other channels observable states with masses  $\simeq (2.6 - 3.6)m_{\text{ng}}^{\text{phys}}$  are present. Some or all of them might be two- or three-particle states.
- (7) No effective energy plateau was found in the channels  $A_1^{+-}$ ,  $A_2^{-+}$ ,  $E^{-+}$  and  $T_1^{-+}$ . However, even in these channels the effective energy at the distance  $t = 0$  is measurable, indicating the possible presence of some heavy, possibly multiparticle states.

We point out that because of the rigorous duality relations for the U(1) lattice gauge theory the same continuum theory can also be obtained as the continuum limit of the following four-dimensional lattice theories: Coulomb gas of monopole loops [46],  $\mathbb{Z}$  gauge theory [47], and non-compact U(1) Higgs

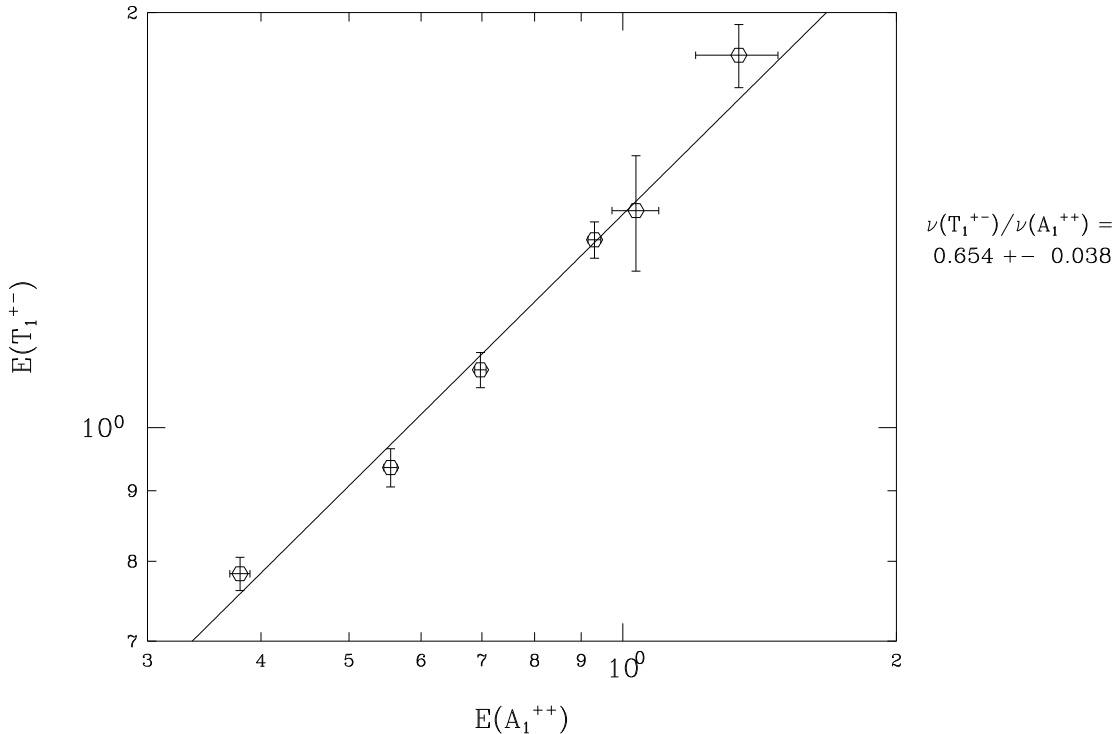


Fig. 12. Different scaling of the two gauge-ball states observed in the Coulomb phase, assuming that the systematic uncertainties are less important in the ratio of the two masses.

model at large negative squared bare scalar mass (frozen four-dimensional superconductor) [2,47]. The last model can be understood as a limit of a theory described by world sheets of Nielsen-Olesen strings [48].

Currently we have no physical picture explaining the observed gauge-ball spectrum. It could be that its understanding might rather come from one of the dual equivalents, for example as the lowest states of a closed Nielsen-Olesen string.

Our results in the Coulomb phase indicate that also here a continuum theory approaching the confinement transition might exist which differs from the free Maxwell theory usually expected in this phase at least in the  $\beta \rightarrow \infty$  limit. However, the masses and the scaling behaviour of the resonances observed in this phase are not yet fully understood. One or even two mass scales might emerge there.

As a spin-off of our study of this phase we confirm the universality [13–15] of the maximal value of the renormalized coupling by obtaining  $\alpha_R^{\max} = 0.19(1)$  in agreement with results in other lattice formulations of the U(1) gauge theory.

Our present work leaves unanswered several questions about the pure U(1) lattice gauge theory and raises many new ones. The major challenge is to understand how the order of the confinement-Coulomb phase transition changes from first at  $\gamma > \gamma_0$  to second at  $\gamma < \gamma_0$ . Is the point  $\gamma_0$  a tricritical point in the sense that several critical lines emerge from it? What are the additional couplings required to reveal this structure? Where are the crossover regions between critical and tricritical scaling behaviour? Are these regions for the  $0^{++}$  state different from those of the other GB states, as required by the  $\mathbf{T}_{\text{ng}}$  and  $\mathbf{T}_{\text{g}}$  scenarios? Or is  $\gamma_0$  an ordinary point of the critical line  $\gamma \leq \gamma_0$ , as would be most natural in the scenario  $\mathbf{C}$ ? Is  $\nu_{\text{ng}}$  a critical or tricritical exponent? A clarification of these questions will require large effort, as  $\gamma$  and possibly some other couplings will have to be varied.

Some arguments can be given for preferring the scenario  $\mathbf{T}_{\text{ng}}$ : (i) It is consistent with some MCRG studies [12]. (ii) Previous results for the string tension [15] and for the massive photon mass [23] at  $\gamma = 0$ , i.e. very close to  $\gamma_0$ , are consistent with the non-Gaussian value. (iii) It is a fairly conventional scenario implying a broad range of dominance of the TCP.

However, the observation of  $\nu \simeq 0.36$  in the finite size scaling analysis even at  $\gamma = -0.5$  [8,9] could be difficult to accommodate in that scenario and prefers scenario  $\mathbf{C}$ . Two different scaling laws at the same critical point might seem to be somewhat exotic. However, the rigorously established results in the three-dimensional pure U(1) gauge theory [37] are strikingly similar. Also there a  $0^{++}$  mass scales faster than the string tension when the gauge coupling vanishes (both scale exponentially). This implies the existence of two different continuum limits. The one with confinement contains a massless scalar, too.

We stress that the existence of the non-Gaussian continuum theory does not depend on which scenario is correct. Only the properties of the  $0^{++}$  state, whether it is light but massive or massless, and whether it couples or not to the other states, depend on the scenario. Thus the fate of the  $0^{++}$  state in the non-Gaussian continuum limit is a challenging question.

The particular scaling behaviour of the  $0^{++}$  GB observed in the present work, in the lattice QCD [38] and in the three-dimensional pure U(1) lattice gauge theory [37] should draw attention towards light scalars in the confining theories.

In the light of so many open questions we should mention the natural caveat of numerical simulations: it might be that only much closer to the phase transition, on lattices much larger than we were able to use, the true behaviour will show up in the future. For example, the scaling of all observables might turn out to be the same at any  $\gamma \leq \gamma_0$ , or the first order transition might reappear even on spherical lattices.

There are several paths which could be pursued with the means currently available:

- Studies similar to the present one at various  $\gamma$  could elucidate the fate of the  $0^{++}$  state and show the cross-over regions if they exist. For this purpose both large negative and some positive  $\gamma$  values will be required.
- It should be possible to investigate the short-range form of the static potential in the confinement phase. This would shed more light on the nontrivial field theory strongly interacting at short distances.
- It would be interesting to find out whether the heavier states observed in the confinement phase are genuine gauge-balls or multi-particle states. If they are resonances, they should be investigated with the appropriate finite size techniques [44,33,45].
- An analysis of the resonances in the Coulomb phase with these techniques would establish their existence and allow to determine the scaling behaviour and continuum limit in this phase as well. The obstacle is the presence of the massless photon, which complicates the analysis devised for theories with a mass gap [44].
- Simulations of the dual  $\mathbb{Z}$  theory might bring further insight into the finite size properties, scaling behaviour of the monopole mass [26], role of boundary conditions, etc.

The pure gauge theory investigated here may not be realized in nature. However, it seems worthwhile to pursue its study, since it widens our understanding of quantum field theories. Our lattice simulations have brought about unexpected results. Further surprises may be waiting.

## Acknowledgements

We thank V. Dohm, M. Göckeler, S. Hands, H.A. Kastrup, D.P. Landau, M. Lüscher, G. Mack, S. Meyer, G. Münster, E. Seiler, P. Weisz, and J. Zinn-Justin for discussions. The computations have been performed on the Cray-YMP and Cray-T90 of HLRZ Jülich. A supplementary Cray-T90 time grant is gratefully acknowledged. J.C., W.F. and J.J. thank HLRZ Jülich for hospitality. The work was supported by DFG.

## References

- [1] K. G. Wilson, *Phys. Rev.* **D10** (1974) 2445; M. Creutz, *Phys. Rev.* **D23** (1981) 1815.
- [2] M. E. Peskin, *Ann. Phys.* **113** (1978) 122.



- [3] T. A. DeGrand and D. Toussaint, *Phys. Rev.* **D22** (1980) 2478.
- [4] B. Berg and C. Panagiotakopoulos, *Phys. Rev. Lett.* **52** (1984) 94.
- [5] J. Jersák, T. Neuhaus, and P. M. Zerwas, *Phys. Lett.* **133B** (1983) 103.
- [6] H. G. Evertz, J. Jersák, T. Neuhaus, and P. M. Zerwas, *Nucl. Phys.* **B251** [FS13] (1985) 279.
- [7] C. B. Lang and T. Neuhaus, *Nucl. Phys.* **B431** (1994) 119.
- [8] J. Jersák, C. B. Lang, and T. Neuhaus, *Phys. Rev. Lett.* **77** (1996) 1933.
- [9] J. Jersák, C. B. Lang, and T. Neuhaus, *Phys. Rev.* **D54** (1996) 6909.
- [10] C. B. Lang and P. Petreczky, *Phys. Lett.* **387B** (1996) 558.
- [11] A. N. Burkitt, *Nucl. Phys.* **B270** [FS16] (1986) 575.
- [12] C. B. Lang, *Phys. Rev. Lett.* **57** (1986) 1828; *Nucl. Phys.* **B280** [FS18] (1987) 255; C. B. Lang and C. Rebbi, *Phys. Rev.* **D35** (1987) 2510.
- [13] J. L. Cardy, *Nucl. Phys.* **B170** [FS1] (1980) 369.
- [14] J. M. Luck, *Nucl. Phys.* **B210** [FS6] (1982) 111.
- [15] J. Jersák, T. Neuhaus, and P. M. Zerwas, *Nucl. Phys.* **B251** [FS13] (1985) 299.
- [16] G. Bhanot, *Nucl. Phys.* **B205** [FS5] (1982) 168.
- [17] R. B. Griffiths, *Phys. Rev.* **B7** (1973) 545; I. D. Lawrie and S. Sarbach, in C. Domb and J. L. Lebowitz, eds., *Phase transitions and critical phenomena*, vol. 9, p. 1 (Acad. Press, New York, 1984).
- [18] H. W. Hamber, *Phys. Rev.* **D24** (1981) 941; A. C. Irving and C. J. Hamer, *Nucl. Phys.* **B235** [FS11] (1984) 358.
- [19] B. Lautrup and M. Nauenberg, *Phys. Lett.* **95B** (1980) 63; G. Bhanot, *Phys. Rev.* **D24** (1981) 461; K. H. Mütter and K. Schilling, *Nucl. Phys.* **B200** [FS4] (1982) 362.
- [20] R. Gupta, M. A. Novotny, and R. Cordery, *Phys. Lett.* **172B** (1986) 86; A. Hasenfratz, *Phys. Lett.* **201B** (1988) 492.
- [21] W. Kerler, C. Rebbi, and A. Weber, *Critical properties and monopoles in U(1) lattice gauge theory*, preprint BU-HEP-96-42, hep-lat/9612001.
- [22] H. G. Evertz, K. Jansen, J. Jersák, C. B. Lang, and T. Neuhaus, *Nucl. Phys.* **B285** [FS19] (1987) 590.
- [23] P. Coddington, A. Hey, J. Mandula, and M. Ogilvie, *Phys. Lett.* **197B** (1987) 191.
- [24] A. Nakamura and M. Plewnia, *Phys. Lett.* **255B** (1991) 274.

- [25] V. G. Bornyakov, V. K. Mitrjushkin, M. Müller-Preussker, and F. Pahl, *Phys. Lett.* **317B** (1993) 596.
- [26] L. Polley and U.-J. Wiese, *Nucl. Phys.* **B356** (1991) 629.
- [27] M. Teper, *Phys. Lett.* **183B** (1986) 345; *Phys. Lett.* **185B** (1987) 121.
- [28] C. Michael and M. Teper, *Nucl. Phys.* **B314** (1989) 347.
- [29] J. Cox, W. Franzki, J. Jersák, C. B. Lang, and T. Neuhaus, *Strongly coupled compact lattice QED with staggered fermions*, in preparation.
- [30] B. Berg and A. Billoire, *Nucl. Phys.* **B221** (1983) 109.
- [31] C. Michael, *Acta Phys. Pol.* **B21** (1990) 119.
- [32] M. Lüscher and U. Wolff, *Nucl. Phys.* **B339** (1990) 222.
- [33] C. R. Gatttringer and C. B. Lang, *Nucl. Phys.* **B391** (1993) 463.
- [34] G. S. Bali, K. Schilling, A. Hulsebos, A. C. Irving, C. Michael, and P. W. Stephenson, *Phys. Lett.* **309B** (1993) 378.
- [35] H. Chen, J. Sexton, A. Vaccarino, and D. Weingarten, *Nucl. Phys. B (Proc. Suppl.)* **34** (1994) 357.
- [36] D. P. Landau, *Phys. Rev.* **B14** (1976) 4054.
- [37] M. Göpfert and G. Mack, *Commun. Math. Phys.* **82** (1982) 545; in J. Honerkamp, K. Pohlmeier, and H. Römer, eds., *Structural elements in particle physics and statistical mechanics*, NATO Adv. Summer Inst., Freiburg 1981, p. 311 (Plenum, 1983).
- [38] U. M. Heller, *Phys. Lett.* **362B** (1995) 123.
- [39] G. Bhanot and R. Dashen, *Phys. Lett.* **113B** (1982) 299.
- [40] T. Blum, C. DeTar, U. M. Heller, L. Karkkainen, and D. Toussaint, *Nucl. Phys. B (Proc. Suppl.)* **42** (1995) 457.
- [41] A. Patrascioiu and E. Seiler, *The problem of asymptotic freedom*, preprint MPI-PHT-96-86, hep-ph/9609292.
- [42] W. Franzki and J. Jersák, *Dynamical fermion mass generation at a tricritical point in strongly coupled  $U(1)$  gauge theory*, in preparation.
- [43] A. Hasenfratz, K. Jansen, J. Jersák, C. B. Lang, H. Leutwyler, and T. Neuhaus, *Z. Phys.* **C46** (1990) 257; A. Hasenfratz et al., *Nucl. Phys.* **B356** (1991) 332.
- [44] M. Lüscher, *Nucl. Phys.* **B354** (1991) 531; *Nucl. Phys.* **B364** (1991) 237.
- [45] M. Göckeler, H. A. Kastrup, J. Westphalen, and F. Zimmermann, *Nucl. Phys.* **B425** (1994) 413.
- [46] T. Banks, R. Myerson, and J. Kogut, *Nucl. Phys.* **B129** (1977) 493.

- [47] J. Fröhlich and P. A. Marchetti, *Europhys. Lett.* **2** (1986) 933; *Commun. Math. Phys.* **112** (1987) 343.
- [48] J. Polchinski and A. Strominger, *Phys. Rev. Lett.* **67** (1991) 1681; M. I. Polikarpov, U.-J. Wiese, and M. A. Zubkov, *Phys. Lett.* **309B** (1993) 133; J. M. Aroca, M. Baig, and H. Fort, *Phys. Lett.* **336B** (1994) 54.

## A Appendix

In this appendix we present two tables with more detailed information about the GB masses. Further data on the effective energies in the confinement phase can be obtained from the authors by e-mail (jersak@physik.rwth-aachen.de).

Table A.1

The effective energies of the  $A_1^{++}$  and  $T_1^{+-}$  gauge-balls with zero momentum in the confinement phase on the time distances  $t/(t+1)$ .

$A_1^{++}$								
Gitter	$\beta$	0/1	1/2	2/3	3/4	4/5	4/6	6/7
16 <sup>3</sup> 32	1.13	1.159(8)	1.09(2)	1.05(6)	0.90(16)	1.1(7)	1.3(11)	
	1.135	1.074(8)	1.023(20)	0.96(7)	1.05(15)	1.2(8)	1.4(11)	
	1.14	0.968(6)	0.914(14)	0.92(3)	1.05(11)	0.7(3)	0.4(3)	0.2(5)
	1.145	0.862(6)	0.815(14)	0.84(4)	0.88(8)	0.76(16)	0.7(3)	0.1(2)
	1.15	0.732(4)	0.692(9)	0.701(15)	0.73(4)	0.77(9)	0.7(2)	0.4(4)
	1.152	0.654(6)	0.618(10)	0.595(15)	0.58(3)	0.60(5)	0.60(11)	0.41(13)
	1.154	0.607(8)	0.559(12)	0.557(18)	0.53(3)	0.50(5)	0.47(9)	0.42(15)
	1.156	0.511(7)	0.472(10)	0.468(15)	0.46(2)	0.48(3)	0.46(5)	0.50(8)
20 <sup>3</sup> 40	1.158	0.412(10)	0.375(12)	0.376(16)	0.38(2)	0.39(3)	0.45(5)	0.48(8)
	1.154	0.588(10)	0.544(13)	0.530(18)	0.53(3)	0.57(6)	0.68(17)	1.1(8)
	1.156	0.533(11)	0.490(17)	0.50(3)	0.51(5)	0.54(9)	0.54(19)	0.5(3)
	1.158	0.410(10)	0.365(14)	0.355(19)	0.35(3)	0.33(4)	0.30(5)	0.28(6)
	1.159	0.306(5)	0.271(6)	0.268(7)	0.262(8)	0.263(10)	0.262(12)	0.260(16)

$T_1^{+-}$								
Gitter	$\beta$	0/1	1/2	2/3	3/4	4/5	4/6	6/7
16 <sup>3</sup> 32	1.13	1.496(6)	1.43(2)	1.32(12)	1.5(4)			
	1.135	1.384(5)	1.314(20)	1.33(8)	1.1(3)	1.4(11)		
	1.14	1.293(5)	1.236(16)	1.24(6)	1.17(17)	0.6(4)	0.3(5)	1.4(9)
	1.145	1.189(4)	1.121(12)	1.08(3)	0.99(10)	0.9(2)	0.4(4)	0.4(5)
	1.15	1.066(4)	0.981(9)	0.97(3)	0.92(6)	0.80(15)	0.6(3)	
	1.152	1.006(4)	0.925(8)	0.903(19)	0.90(6)	0.94(16)	1.1(9)	
	1.154	0.950(4)	0.863(8)	0.843(18)	0.87(4)	0.87(12)	1.2(5)	0.4(7)
	1.156	0.798(4)	0.738(8)	0.732(14)	0.75(3)	0.73(5)	0.71(14)	1.0(5)
20 <sup>3</sup> 40	1.158	0.668(4)	0.601(6)	0.588(10)	0.564(17)	0.56(3)	0.57(6)	0.54(10)
	1.154	0.956(5)	0.862(13)	0.83(3)	0.76(5)	0.73(15)	0.5(2)	0.6(6)
	1.156	0.779(6)	0.729(11)	0.74(3)	0.73(5)	0.81(11)	0.7(2)	0.8(5)
	1.158	0.676(5)	0.624(9)	0.624(18)	0.60(3)	0.60(5)	0.58(11)	0.7(2)
	1.159	0.5933(19)	0.528(3)	0.518(4)	0.510(6)	0.528(11)	0.540(16)	0.53(3)

Table A.2

Masses for all  $R^{PC}$  combinations obtained from operators with zero and smallest nonvanishing momentum.

$R^{PC}$	$\frac{p_z L}{2\pi}$	$16^3 32$						
		$\beta = 1.13$	$\beta = 1.135$	$\beta = 1.14$	$\beta = 1.145$	$\beta = 1.15$	$\beta = 1.152$	$\beta = 1.154$
$A_1^{++}$	0	1.08(7)	1.02(8)	0.95(4)	0.85(5)	0.721(20)	0.599(19)	0.55(2)
	1	1.27(11)	1.25(8)	1.00(4)	0.80(3)	0.70(3)	0.66(2)	0.566(20)
$A_1^{+-}$	0			2.3(12)	3.9(18)	2.1(10)	1.8(4)	2.1(6)
$A_1^{-+}$	0	2.6(17)				2.4(6)	2.7(17)	2.7(8)
$A_1^{--}$	0	3(2)		1.0(11)	1.4(12)	2.1(7)	1.8(14)	2.1(7)
$A_2^{++}$	0	2.2(14)	2.5(16)		5(4)	3.5(19)	5(3)	1.9(4)
$A_2^{+-}$	0	1.5(3)	1.6(3)	1.20(10)	1.19(9)	1.00(4)	0.95(5)	0.92(4)
$A_2^{-+}$	0	1.3(13)			1.9(11)	3(2)	5(3)	
$A_2^{--}$	0		3.2(20)		11(8)	3.6(17)		1.2(6)
$E^{++}$	0	2.2(5)	1.8(9)	3.0(5)	2.6(3)	2.10(14)	1.88(12)	1.74(8)
	1	1.4(14)	2.8(7)	2.5(3)	2.6(3)	2.25(17)	2.04(13)	1.99(11)
$E^{+-}$	0	1.65(19)	1.29(12)	1.31(11)	1.05(6)	0.96(4)	0.91(3)	0.84(3)
$E^{-+}$	0		6(2)	1.2(16)	1.9(9)	4.0(16)	2.9(6)	3.0(7)
$E^{--}$	0	10(4)	7(5)		5(3)	2.2(6)	2.3(6)	2.7(6)
$T_1^{++}$	0		4(2)	10(5)		4(2)	9(4)	1.4(9)
	1		5(2)			2.3(12)		1.4(5)
$T_1^{+-}$	0	1.43(15)	1.42(9)	1.29(7)	1.11(4)	1.00(3)	0.93(2)	0.87(2)
	1	1.58(19)	1.25(16)	1.50(12)	1.16(9)	1.01(4)	0.85(4)	0.88(4)
$T_1^{-+}$	0	2.4(15)	2.5(15)	1.4(8)	5(3)	13(5)	1.8(9)	4(2)
	1	1.7(4)	1.0(3)	1.13(11)	0.76(7)	0.73(3)	0.67(4)	0.59(3)
$T_1^{--}$	0	2.6(17)	4(2)	30(13)	1.6(8)	2.7(11)	1.7(7)	3.9(15)
	1	0.8(14)	1.4(6)	1.6(11)		2.7(14)	4(2)	1.7(14)
$T_2^{++}$	0	3.6(11)	3.3(6)	3.1(3)	2.6(2)	2.13(11)	1.91(8)	1.85(6)
	1	4.8(20)	2.5(4)	4.4(16)	2.3(2)	2.2(2)	1.95(14)	1.73(8)
$T_2^{+-}$	0	1.48(14)	1.44(10)	1.25(8)	1.07(5)	0.99(3)	0.93(2)	0.86(2)
	1	1.37(19)	1.14(14)	1.45(14)	1.28(9)	0.99(5)	0.92(5)	0.83(4)
$T_2^{-+}$	0	6(3)	2.6(12)	2.3(10)	1.7(14)	3.9(12)	2.4(4)	2.1(2)
	1			1.7(4)	1.8(13)	3.0(9)	2.4(6)	2.4(4)
$T_2^{--}$	0			7(3)	19(10)	7(4)	2.8(17)	2.8(7)
	1	2.9(19)	3(2)	1.0(4)	1.4(7)	0.9(2)	1.09(15)	0.86(9)

Table A.3  
Continuation of table A.2

$R^{PC}$	$\frac{p_z L}{2\pi}$	$16^3 32$		$20^3 40$			
		$\beta = 1.156$	$\beta = 1.158$	$\beta = 1.154$	$\beta = 1.156$	$\beta = 1.158$	$\beta = 1.159$
$A_1^{++}$	0	0.47(2)	0.39(2)	0.54(2)	0.51(4)	0.34(3)	0.265(9)
	1	0.459(19)	0.33(3)	0.51(2)	0.43(3)	0.31(2)	0.293(6)
$A_1^{+-}$	0	1.88(18)	1.70(11)	2.3(7)	1.8(9)	1.6(2)	1.65(4)
$A_1^{-+}$	0	2.7(6)	1.72(14)	11(6)	1.9(6)	2.0(3)	1.49(3)
$A_1^{--}$	0	2.6(7)	1.73(20)	1.6(14)	1.2(3)	1.3(4)	1.47(4)
$A_2^{++}$	0	2.3(13)	2.0(2)	4(2)	2.2(8)	2.1(3)	1.70(5)
$A_2^{+-}$	0	0.79(3)	0.61(2)	0.84(6)	0.71(4)	0.62(3)	0.529(10)
$A_2^{-+}$	0		1.5(4)	1.0(17)	0.8(9)		2.8(4)
$A_2^{--}$	0	2.4(9)	1.8(2)	1.9(12)	2.1(10)	1.8(4)	1.46(5)
$E^{++}$	0	1.56(5)	1.22(2)	1.70(9)	1.60(8)	1.30(5)	1.098(11)
	1	1.67(7)	1.47(4)	1.90(12)	1.80(13)	1.42(6)	1.193(12)
$E^{+-}$	0	0.76(2)	0.590(17)	0.85(4)	0.76(4)	0.62(3)	0.510(8)
$E^{-+}$	0	2.1(3)	1.63(10)	1.9(13)	1.5(2)	1.66(15)	1.58(3)
$E^{--}$	0	2.02(19)	1.78(10)	1.6(4)	2.1(4)	1.77(15)	1.56(3)
$T_1^{++}$	0	0.9(7)	2.4(3)	2.8(15)	10(5)	1.8(14)	1.94(6)
	1	3.0(11)	1.9(3)	6(3)	1.4(8)	2.9(12)	1.89(9)
$T_1^{+-}$	0	0.751(16)	0.588(12)	0.83(3)	0.76(4)	0.63(2)	0.524(5)
	1	0.76(3)	0.64(2)	0.78(5)	0.71(3)	0.62(2)	0.522(6)
$T_1^{-+}$	0	1.8(2)	1.9(4)	2.5(14)		1.6(3)	2.22(9)
	1	0.45(2)	0.33(3)	0.51(3)	0.45(4)	0.33(2)	0.295(8)
$T_1^{--}$	0	1.81(17)	1.62(9)	3.0(15)	1.9(4)	1.82(16)	1.50(3)
	1	1.7(2)	2.09(18)	2.3(8)	1.6(8)	1.7(2)	1.59(3)
$T_2^{++}$	0	1.68(5)	1.29(3)	1.75(9)	1.53(6)	1.26(4)	1.077(8)
	1	1.64(6)	1.34(4)	1.66(12)	1.55(10)	1.31(5)	1.209(12)
$T_2^{+-}$	0	0.761(16)	0.591(12)	0.85(3)	0.76(4)	0.63(2)	0.525(7)
	1	0.75(3)	0.60(2)	0.88(6)	0.75(5)	0.61(3)	0.533(9)
$T_2^{-+}$	0	1.68(13)	1.78(8)	2.2(3)	1.9(3)	1.79(13)	1.69(3)
	1	1.87(20)	1.59(9)	1.8(3)	1.8(4)	1.42(11)	1.38(2)
$T_2^{--}$	0	1.93(20)	1.99(14)	4(2)	4(2)	1.91(19)	1.74(5)
	1	0.84(6)	0.65(4)	0.68(16)	0.63(7)	0.71(6)	0.548(13)